Tectonics

RESEARCH ARTICLE
10.1029/2020TC006116

Key Points:
- The Apulia Swell, an offshore foreland enclosed between two contractional domains, is undergoing extension since the Early Pleistocene
- Extension in the Apulia Swell is accommodated by the South Apulia Fault System, a 100-km-long and 12-km-wide structure
- The South Apulia Fault System has a slip rate of 0.2–0.4 mm/yr and could have caused the 20 February 1743, magnitude 6.7, earthquake

Supporting Information:
- Supporting Information S1
- Table S1
- Table S2
- Table S3
- Table S4
- Table S5
- Table S6

Correspondence to:
F. E. Maesano,
francesco.maesano@ingv.it

Citation:
Maesano, F. E., Volpi, V., Civile, D., Basili, R., Conti, A., Tiberti, M. M., et al. (2020). Active extension in a foreland trapped between two contractional chains: The South Apulia Fault System (SAFS). *Tectonics*, *39*, e2020TC006116. https://doi.org/10.1029/2020TC006116

Received 4 FEB 2020
Accepted 8 JUN 2020
Accepted article online 11 JUN 2020

Author Contributions:
Data curation: F. E. Maesano, V. Volpi, D. Civile, D. Accettella, R. Conte, F. Zgur
Validation: F. E. Maesano, V. Volpi, D. Civile, R. Basili, A. Conti, M. M. Tiberti, G. Rossi
Writing – review & editing: F. E. Maesano, V. Volpi, D. Civile, R. Basili, A. Conti, M. M. Tiberti, G. Rossi

Active Extension in a Foreland Trapped Between Two Contractional Chains: The South Apulia Fault System (SAFS)

F. E. Maesano[1], V. Volpi[2], D. Civile[2], R. Basili[1], A. Conti[3], M. M. Tiberti[1], D. Accettella[2], R. Conte[2], F. Zgur[2], and G. Rossi[2]

[1]Istituto Nazionale di Geofisica e Vulcanologia, Rome, Italy, [2]Istituto Nazionale di Oceanografia e Geofisica Sperimentale (OGS), Trieste, Italy, [3]Dipartimento di Scienze della Terra, Università Sapienza di Roma, Rome, Italy

Abstract The response of continental forelands to subduction and collision is a widely investigated topic in geodynamics. The deformation occurring within a foreland shared by two opposite-verging chains, however, is uncommon and poorly understood. The Apulia Swell in the southern end of the Adria microplate (Africa-Europe plate boundary, central Mediterranean Sea) represents one of these cases, as it is the common foreland of the SW verging Albanides-Hellenides and the NE verging Southern Apennines merging into the SSE verging Calabrian Arc. We investigated the internal deformation of the Apulia Swell using multiscale geophysical data: multichannel seismic profiles recording up to 12-s two-way time (TWT) for a consistent image of the upper crust; high-resolution multichannel seismic profiles, high-resolution multibeam bathymetry, and CHIRP profiles acquired by R/V OGS Explora to constrain the Quaternary geological record. The results of our analyses characterize the geometry of the South Apulia Fault System (SAFS), a 100-km-long and 12-km-wide structure attesting an extensional (and possibly transtensional) response of the foreland to the two contractional fronts. The SAFS consists of two NW-SE right-stepping master faults and several secondary structures. The SAFS activity spans from the Early Pleistocene through the Holocene, as testified by the bathymetric and high-resolution seismic data, with long-term slip rates in the range of 0.2–0.4 mm/yr. Considering the position within an area with few or none other active faults in the surroundings, the dimension, and the activity rates, the SAFS can be a candidate causative fault of the 20 February 1743, *M* 6.7, earthquake.

1. Introduction

The central Mediterranean region is known for being a puzzle of microplates interwoven with a network of thrust belts, back-arc basins, and transfer zones. The Adria microplate, which is almost entirely under the Adriatic and Ionian Seas, lies in the middle of this puzzle (Figure 1a). The southern end of the Adria microplate, composed by the Salento Peninsula (to the north) and the Apulia Swell (to the south), is the Neogene-Quaternary foreland (herein referred to as Apulian Foreland) of two opposite-verging chains: the SW verging Albanides-Hellenides and NE verging Southern Apennines merging southwardly with the SSE verging Calabrian Arc. The Adria microplate mainly consists of the Apulia carbonate platform that is a block of continental crust (Critelli, 2018) which preserved, in its southwestern part, the paleomargin with the Ionian oceanic crust that subducted under the Calabrian Accretionary Wedge, to the west, and the Hellenic Arc, to the east. Several authors have analyzed the structural setting of the Apulia Foreland (Argnani et al., 2001; Billi et al., 2007; Butler, 2009; Catalano et al., 2000; Del Ben, 2009; Del Ben et al., 2015; Doglioni et al., 1999; Finetti & Del Ben, 2005; Gambini & Tozzi, 1996; Milia et al., 2017; Nicolai & Gambini, 2007; Teofilo et al., 2018; Tondi et al., 2005; Volpi et al., 2011, 2017) and all together point out that it is affected by E-W strike-slip faults in the northern part (Mattinata-Gondola Fault, MGF), and NW-SE trending extensional structures in the Salento Peninsula and Apulia Swell (Figure 1b). The role, age, and origin of these tectonic lineaments are a matter of debate. The Apulia Foreland is considered to be the peripheral bulge produced by flexural bending due to the loading of the two confronting chains mentioned above (Critelli, 2018; Critelli et al., 2017; Moretti & Royden, 1988). For several authors, this bending was responsible for an extensional tectonic regime developed during the Pliocene-Quaternary and thereby generating NW-SE normal faults (Argnani et al., 2001; Ciaranfi et al., 1988; Finetti & Del Ben, 2005).

10.1029/2020TC006116

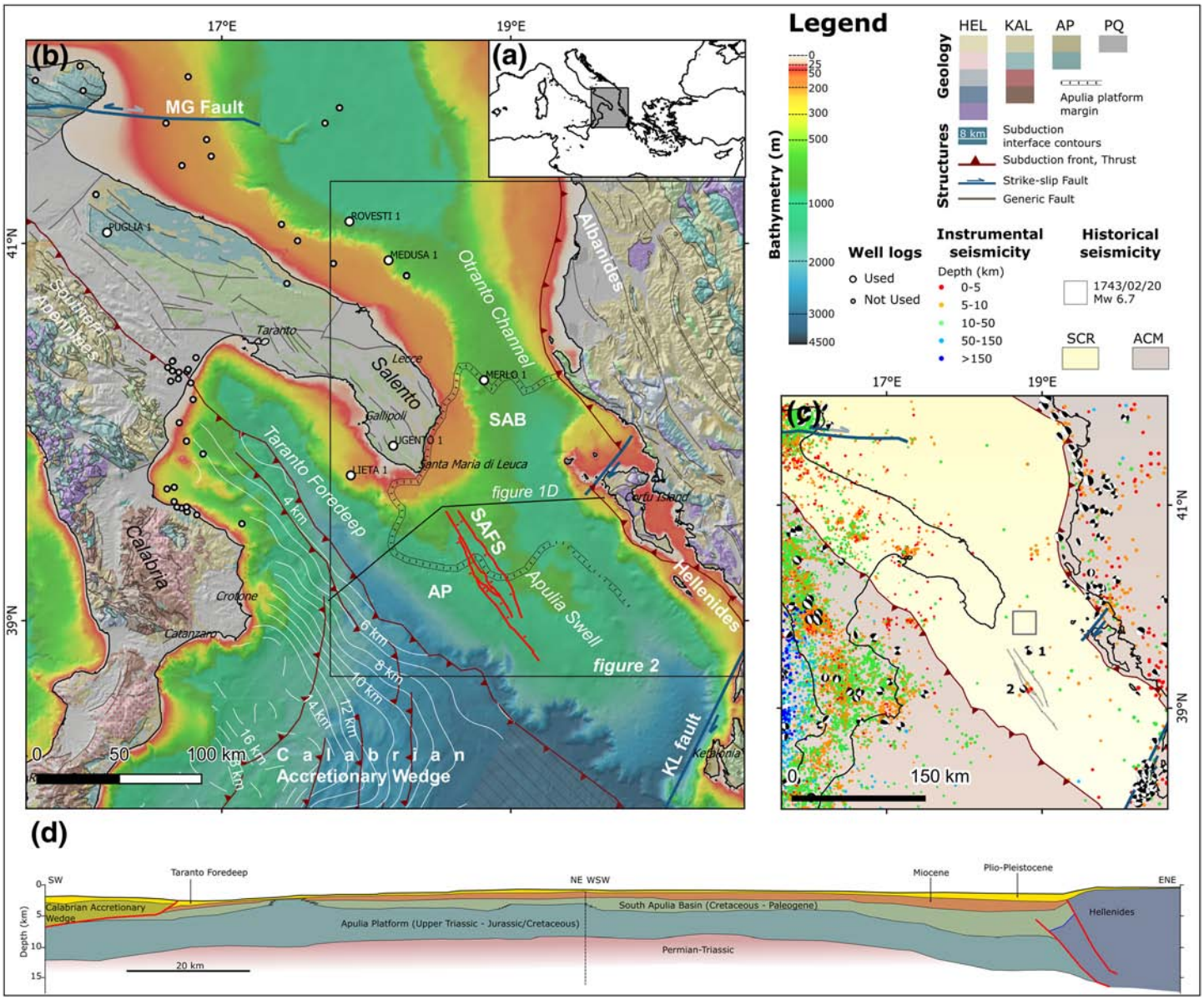

Figure 1. (a) Location of the study area. (b) Geological framework. SAB: South Apulia Basin; AP: Apulia Platform, KL fault: Kefalonia Lefkada fault, MG fault: Mattinata Gondola fault; CA subduction: Calabrian subduction contours from Maesano et al. (2017), Calabrian Accretionary Wedge thrusts from Minelli and Faccenna (2010), SAFS: South Apulia Fault System. Well logs position from ViDEPI (http://www.videpi.com). Geological background reproduced with the permission of the OneGeology, all rights reserved (http://www.onegeology.org/portal/home.html): HEL = Hellenides units, KAL = Calabrian units, AP = Apulian unit, PQ Pliocene-Quaternary deposits. (c). Seismotectonic sketch. Instrumental seismicity covers the time interval 2005–2016 (ISIDe Working Group, 2007). Centroid Moment Tensors (CMT) for the time interval 1976–2015 (Pondrelli & Salimbeni, 2006). Historical seismicity of the study area (20 February 1743 *Mw* 6.68) from CPTI15 (Rovida et al., 2016). SCR = Stable continental region; ACM = Active compressive margin; (1) focal mechanism from first motion of the 20 October 1974 earthquake, *Ml* 5.1, *Mw* 5.02, strike/dip/rake 200/59/160, 300/73/32, trend/plunge of *P* axis 67/10, *T* axis 164/33, and *B* axis 322/55 (Favali et al., 1990); (2) CMT of the 5 September 2014 earthquake, *mb* 4.1, *Mw* 4.06, strike/dip/rake 334/39/−56, 113/58/−114, trend/plunge of *P* axis 335/66, *T* axis 220/10, and *B* axis 126/20 (Pondrelli & Salimbeni, 2006). (d) Schematic crustal geological section across the study region based on CROP data.

Di Bucci et al. (2011) suggested that after the Late Pleistocene, a sort of radial extension is detectable, indicating a doming of the foreland area replacing the Middle Pleistocene SW-NE extension. The doming is the consequence of the coexistence of SW-NE contraction due to the advancing two chains combined with the northward push of the African plate.

In this work, we focus on the Apulia Swell (Figure 1b), a long-wavelength ridge, elongated NW-SE. Based on borehole data, its Meso-Cenozoic ~8-km-thick shallow-water carbonate succession consists of Paleogene

transgressive clastic carbonate deposits, Cretaceous limestones, Jurassic dolostones, and late Triassic anhydrite-dolomites (Anidriti di Burano Formation) resting unconformably on more than 1,000 m of Early Triassic-Permian terrigenous deposits (Ricchetti et al., 1988). Offshore seismic data highlight the presence of three seismic facies within the Mesozoic carbonate succession of the Apulia Swell (Volpi et al., 2017): a reflection-free seismic facies, assigned to a massive carbonate platform succession; a well-layered seismic facies linked to the presence of an intraplatform basin, that is, the South Apulia Basin, originated since Jurassic time (Del Ben et al., 2015); and a seismic facies characterized by discontinuous, low- to moderate-amplitude reflectors interpreted as a platform-to-basin transition zone. Above this carbonate succession there are two additional sedimentary bodies (Butler, 2009; Volpi et al., 2017): an upper Miocene succession, bounded to the top by the Messinian unconformity and consisting of discontinuous and high-amplitude reflectors; and a Pliocene-Quaternary sequence characterized by high-amplitude, continuous, and subparallel reflectors which includes a lower semitransparent seismic facies associated with the Lower Pliocene pelagic deposits of the Trubi Formation.

The NW-SE extensional faults that affect the Salento Peninsula continue offshore, as highlighted by many authors (Argnani et al., 2001; Butler, 2009; Del Ben et al., 2010; Milia et al., 2017; Volpi et al., 2017). The interpretation of seismic profiles by Butler (2009) provided an upper Miocene-lower Pliocene age for these normal faults, whereas Volpi et al. (2017) suggested that the activity of these faults occurred after the lower Pliocene. Some of these normal faults displace the seafloor, and Merlini et al. (2000) proposed that they are active and responsible for the seismicity of the Salento Peninsula. Conversely, Argnani et al. (2001) suggested that the seismicity recorded in the Salento area may be generated by an inner-arc contraction within the Adriatic upper crust, whereas outer-arc extension would have originated grabens bounded by NW-SE normal faults. For Milia et al. (2017), the NW trending normal faults affect the early Lower Pleistocene deposits and are sealed by younger deposits. Besides, Milia et al. (2017) contend that since middle Pleistocene, a compressional event produced the Apulia uplift associated with large folds and basement-involved reverse faults that are active in the eastern sector of Apulia. Galli and Naso (2008) interpreted the NW trending normal faults as minor faults of a limited length and confined within the upper 2–3 km of the crust. Their interpretation, however, is based on bathymetric and shallow subsurface geophysical data, which can image neither the lateral continuity nor the depth-wise propagation of such faults.

Seismicity within the Apulia Foreland is scarce and sparse, in agreement with the characteristics of a stable continental region (Figure 1c). Nonetheless, this area hosted an M 6.7 earthquake on 20 February 1743 and a small sequence in 1974 (Rovida et al., 2016). Recently (2013–2014), some small events were recorded by the seismic network in the Apulia Swell with magnitude range 3.1–4.1 and depth between 5 and 10 km (ISIDe Working Group, 2007; Pondrelli & Salimbeni, 2006). The available focal mechanisms for the 1974 seismic sequence (Favali et al., 1990; Muço, 1994) suggest a strike-slip kinematics with left-lateral component of movement on NW-SE planes (main events of the 20 October 1974), whereas the main event of the 2013–2014 seismic sequence suggest an extensional mechanism with a small left lateral component along NW-SE planes (Figure 1c). Also, a deep-seated (hypocenter depth of 49 km) oblique compressive event was recorded on 23 November 1974. Argnani et al. (2001) suggest that the earthquakes recorded in this area, including the 1743 event, can be the direct consequence of contraction at depths greater than 10 km, due to the buckling of the Apulia Swell that generates normal faulting at the surface. The 20 February 1743 earthquake heavily damaged the Salento Peninsula and the Ionian Islands (Greece) and was widely felt in all the Ionian and Adriatic regions (Guidoboni et al., 2019; Locati et al., 2016; Nappi et al., 2017). It also caused a tsunami that was observed in the Brindisi harbor (Guidoboni et al., 2019) and is supposed to have affected the southeastern coast of the Salento Peninsula (Mastronuzzi et al., 2007). However, its actual location is poorly known because of the dearth of macroseismic data in the near field. Several location alternatives are available: in the Ionian Sea (Rovida et al., 2016), onshore in the Salento Peninsula (Guidoboni et al., 2019), or close to Corfu Island (Milia et al., 2017). As regard the tectonic source of this earthquake, Galli and Naso (2008), following Argnani et al. (2001) and based on macroseismic field analysis, ascribe it to a still unknown deep reverse fault related to contraction at depth in the Apulia Swell, whereas Milia et al. (2017) suggested that the source might be a thrust fault located in the outermost front of the Hellenides Chain.

The interpretation of a multiscale data set presented in this study suggests that the extensional structural elements previously recognized in the Apulia Swell pertain to a major active fault system, herein referred to as the South Apulia Fault System (SAFS), that can be followed for a length of at least 100 km (Figure 1b). We

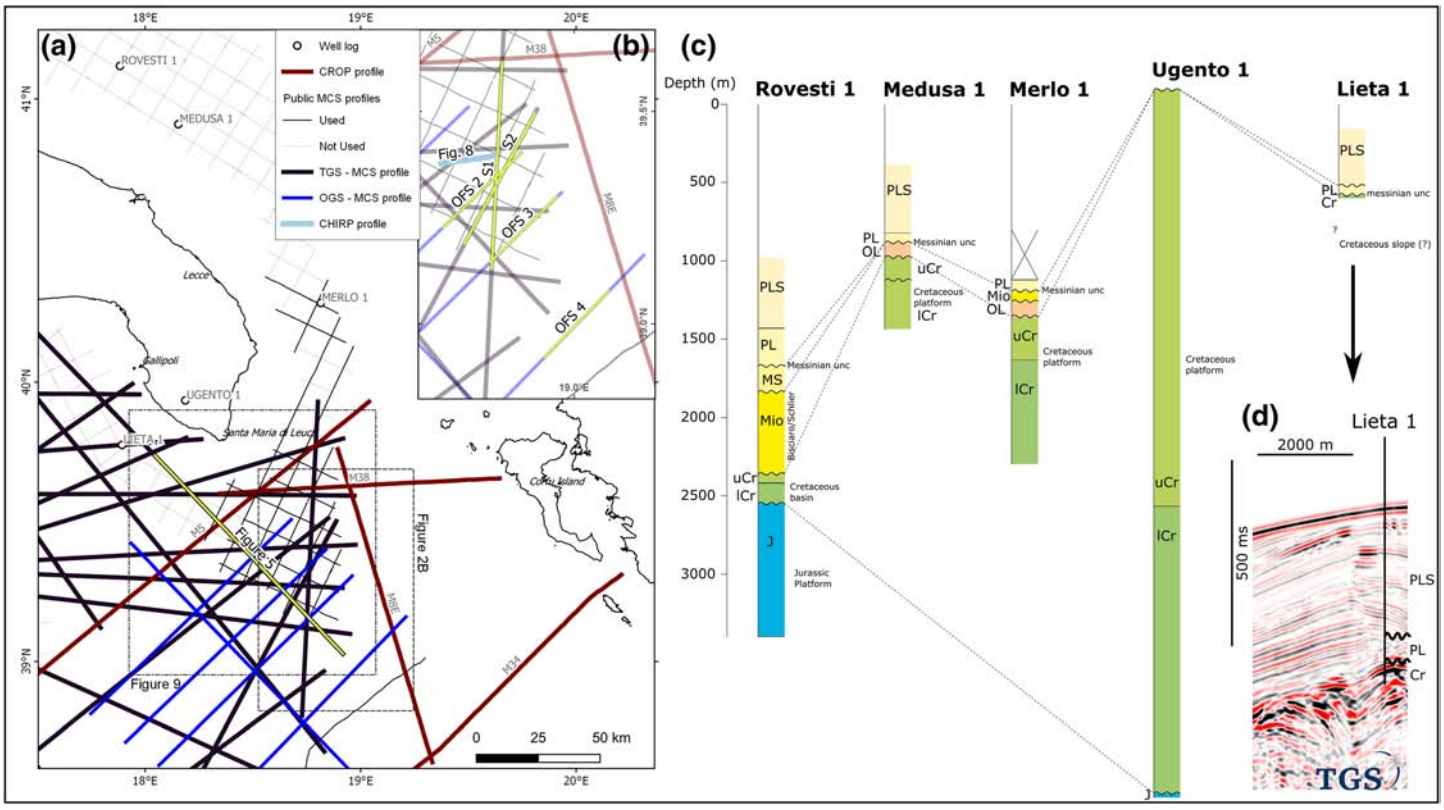

Figure 2. (a) Overview of the subsurface data available in the Apulia Foreland. (b) Close up of the study region with the segments of the seismic profiles shown in Figures 6 and 7 highlighted in yellow. (c) Schematic view of boreholes stratigraphy in the Apulia Foreland (see panel a for location) and correlation, borehole data from ViDEPI database (http://www.videpi.com), (d) tie of seismic profile with Lieta 1 well. PLS = Pleistocene; PL = Pliocene, MS = Messinian, MIO = Miocene, OL = Oligocene, Cr = Cretaceous s.l., uCr = upper Cretaceous, lCr = lower Cretaceous, and J = Jurassic.

were also able to constrain the geometry and to estimate the activity rates of this fault system and to make some inferences on its kinematics. The presence of such an important fault system within a relatively stable continental region—or at least a region not directly involved in the orogenic process—poses more general questions on the intraplate deformation of this part of the Adria microplate and on how to treat such areas in earthquake hazard studies.

2. Data and Method

The seismic data used in this study (Figure 2a) integrate public available multichannel reflection profiles (ViDEPI database, Italian Ministry of the Economic Development, http://www.videpi.com) and CROP profiles (http://www.crop.cnr.it/en/) with multichannel seismic profiles of the GT08 and CA99 surveys confidentially provided by TGS and seismic data acquired by R/V OGS Explora during several geophysical campaigns. The OGS data set includes five multichannel seismic profiles (OFS_10 data set) acquired in 2010, high-resolution CHIRP profiles collected in the framework of the FASTMIT research project in 2018, and ~12.5 km^2 of morphobathymetric data, in a depth range from 630 to 3,450 m below sea level, acquired in 2003, 2005, 2010, and 2018. The technical parameters of the acquisition and processing of the various data sets are provided in Table 1, and their location is shown in Figure 2.

The morphobathymetric data were acquired with R/V OGS Explora hull-mounted Reson® SeaBat 8,150, 7,150, 8,111. They operate at a frequency of 12 kHz (7150 and 8150) and 100 kHz (8111) with a 150° across-track and 1.5° along-track swath. Three integrated D-GPS systems ensured navigation. The collected data, logged through the PDS2000® acquisition software, were corrected for ship's motion, navigation, sound velocity, and tides. The data processing consisted of three actions: (1) calibration of data (time, pitch, roll, and yaw), (2) correction of depth measurements using sound velocity profile of the seawater measured at

Table 1
Characteristics, Including Acquisition Parameters, of the Geophysical Surveys Shown in Figure 2a

	TGS MCS	CROP	OGS MCS	Videpi
Number of lines	18	4	4	28
Total length (km)	1,789	527	429.9	738
Record length (s)	6–12	17–20	6.6	6.6
Source type	Airgun array	High-pressure airgun	GI-GUN Sercel	Steam gun
Source power	3,410–5,000 c.i.	140 bar	140 atm	—
Source depth (m)	6	6	4 ± 0.5	5
Streamer depth (m)	8	12	5 ± 0.5	19
Streamer length (m)	6,000–8,100	4,500	1,500	2,400
Shotpoint interval (m)	25	62.5	50	50
Group interval (m)	12.5	25	50	50

Note. MCS = multichannel survey.

different locations,and (3) manual editing to remove errors in the navigation positions and residual spikes. The resulting Digital Terrain Model (with a grid cell size of 50 × 50 m) was then edited (removal of residual spikes) and filtered.

CHIRP data were acquired with a hull-mounted Benthos Teledyne® Chirp III DSP-665, characterized by sweeps ranging from 2 to 7 kHz (the vertical resolution is in the order of decimal centimeters). The SwanPro® software was used to collect the data, which were processed using VISTA Schlumberger software to adjust for the time shift and to balance the seismic amplitude.

The OGS multichannel seismic profiles were acquired using a 1,500-m-long Sercel digital streamer with 120 channels spaced 12.5 m apart, corresponding to an effective horizontal sampling of 6.25 m in the stacked section. The seismic source consisted of two expanded volume of 355 $in.^3$ (8 L) GI guns organized in a 2-m-long linear array and fired in harmonic mode, in order to provide a good quality signature by reducing the bubble effect, while preserving a sufficient amount of emitted acoustic energy. The source was towed at a depth of 4 m, the streamer at 5 m, with the first ghost effect related frequency notch occurring at around 150 Hz. The shot point interval was 25 m, with a resulting fold coverage of 30 traces for each investigated common depth point. The processing consisted in the following steps: data reformatting from SEGD field format to Vista processing package internal format, trace editing, amplitude recovery, sort from shot point to common depth point domain, velocity analysis every 400 common midpoints (around 2,500 m), Normal Move Out correction, and stack and time migration. After a first evaluation of the preliminary results, specific velocity analysis (based on velocity spectra and common velocity stack) was later conducted on selected locations to improve the velocity model along the profiles and better assist the interpretation.

The data set provided by TGS, CNR-ISMAR (CROP data set), and ViDEPI were already processed, and we did not perform any further elaboration on them. The TGS data set is constituted by 18 multichannel seismic reflection profiles with variable record depth from 6 to 12 s and prevalent orientation NW-SE, ENE-WSW, N-S, and E-W for a total length, within the study area, of 1,789 km. CROP profiles crossing the Apulia Swell (*M*5, *M*38, *M*8E, and *M*34) cover a length of 527 km within the study area. These profiles have low resolution in the shallow interval but very high penetration (up to 20 s) and thus were used to constrain the general crustal geometry of the Apulia Swell (Figure 1d), also considering their interpretation provided in previous studies (Del Ben et al., 2015; Finetti & Del Ben, 2005; Merlini et al., 2000; Milia et al., 2017). Publicly available ViDEPI profiles generally have a low resolution and very poor definition of deep-seated reflectors and thus were used only to extend the interpretation of the shallower horizons in the sector located between higher-quality profiles.

The seismic interpretation was performed using IHS Kingdom Suite software and MOVE (Petroleum Expert Ltd.). The seismic-well correlation was performed to calibrate seismic horizons in depth. Five hydrocarbon exploration wells, one of them located onshore (Ugento 1), have been considered (Figure 2a), retrieved from the ViDEPI database (Figure 2c). The final results of the seismic interpretation are isochron maps in two-way time (sec) obtained by interpolating the seismic horizons picked on the seismic sections. Beforehand, each horizon was subdivided into different blocks separated by the major faults that were

Table 2
Velocity Model Derived From the Analysis of the Medusa 1 Sonic Log (See Supporting Information Figure S1 for Details)

Layer	Interval velocity (m/s)
Water	1,500
Pliocene-Holocene	2,090
Miocene	3,250
Upper Cretaceous-Oligocene	3,650
Jurassic-Lower Cretaceous	5,700

previously correlated among different seismic profiles. Inside each block, a triangular Delaunay interpolation was applied within a grid with an average spacing of 500 × 500 m.

The time-to-depth conversion was based on the velocity model derived from the analysis of the sonic log of the Medusa 1 well and reported in Table 2; the velocity model was calibrated considering the average velocity derived from the sonic log within each stratigraphic interval. The sonic logs were digitized using the Neuralog software and are made available in the supporting information (Figure S1). The time-to-depth conversion was applied to the 3-D surfaces using the simple interval velocities of Table 2 with the tool Vel-IO 3-D (Maesano & D'Ambrogi, 2017) specifically developed for the time-depth conversion of complex 3-D surfaces. We used the depth-converted horizons to analyze and discuss the thickness of pretectonic, syntectonic, and postectonic units, to evaluate the age of inception of the faults and to calculate their throw rates.

3. Results

The interpretation of the multiscale geophysical data set allowed us to identify and characterize a major NW-SE oriented faults system, which extends for a total length of at least 100 km in the Apulia Swell. This system is mainly composed of extensional faults collectively named SAFS. In the next paragraphs, we will describe the SAFS internal geometry and the geomorphic features at the seafloor through the analysis of the bathymetry and the interpretation of the 2-D seismic profiles.

3.1. Morphobathymetric Features

The bathymetric map obtained from the integration of the high-resolution multibeam data acquired by OGS with the morphobathymetric data available from EMODnet Portal (http://www.emodnet-geology.eu) emphasizes the main physiographic elements of the study area (Figure 3a). The Apulia Swell lies in the center as a relative bathymetric high limited by the Taranto foredeep channel to the west and the Kerkira basin to the east. To the north, the Apulia continental platform is separated from the offshore area by a relatively steep scarp, characterized in its upper portion by evident failure scars and by an NNW-SSE trending ridge in the deepest sector. At the base of the slope, the presence of mass-wasting deposits produces the rough morphology of the seafloor. To the west of the Taranto foredeep channel, the seabed shows an irregular morphology characterized by ridges and troughs that are the expression of the allochthonous thrust sheets of the Calabrian accretionary wedge. To the east, a steep and incised slope connects the Hellenic continental platform to the Kerkira basin, while to the south, the transition between the Apulia Swell and the Ionian abyssal plane occurs through a steep and irregular scarp. The central part of the Apulia Swell (close-up view in Figure 3b) is affected by a set of NW-SE oriented structural lineaments that start from the base of the continental shelf. These lineaments bound two tectonic depressions here named Northern Basin and Southern Basin (Figure 3b). The Northern Basin is 12 km wide and 45 km long. The Southern Basin is 5.5 km wide, and it extends for at least 40 km in length. The two basins are arranged in an en echelon fashion and are separated by a 25-km-long ridge here named Central Horst.

Each NW trending tectonic lineament belongs to SAFS has been labeled with the acronym SAF followed by a serial number, increasing from north to south. The analysis of the SAFS lineaments was carried out through 27 morphobathymetric profiles crossing the principal axis of the two basins orthogonally. The morphobathymetric interpretation is shown in Figure 3b, whereas the results of the analysis for a selected number of profiles are shown in Figure 4 (the entire data set is provided in the supporting information Figure S2).

SAF1 is a 30-km-long lineament, which bounds the Northern Basin to the west and delimits the eastern side of the Central Horst (west side up). A local change in the SAF1 trend is visible in its southern part where the Central Horst shows the maximum topographic relief characterized by a fault scarp up to 330 m high (Figures 4c and S2, Profile 12). SAF2 can be followed discontinuously for about 50 km. It bounds the eastern side of the Northern Basin (east side up) that is characterized by a less pronounced relief with a fault scarp height of 130 m (Figure 4b, Profile 6). SAF3 shows a slightly curved trace bounding the Central Horst to the west (east side up) and affecting the northern termination of the Southern Basin. This lineament follows an

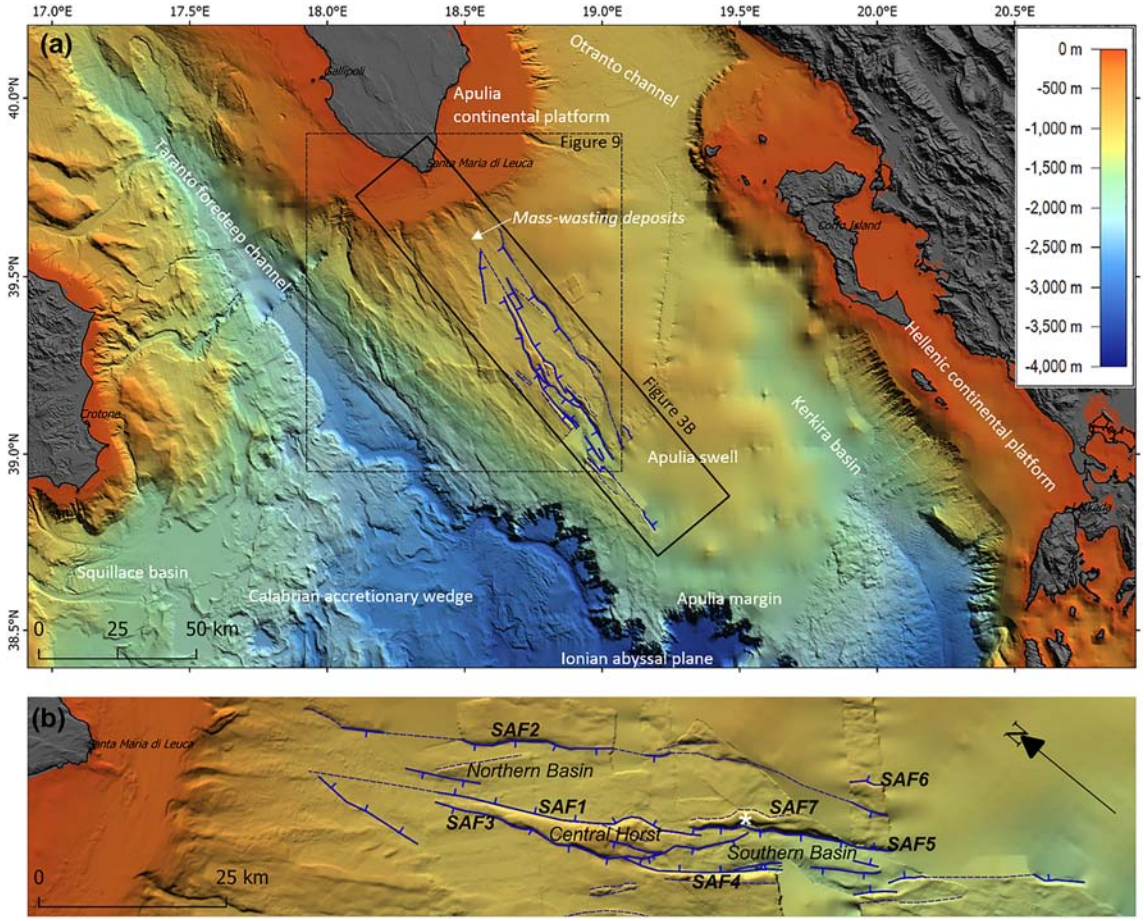

Figure 3. (a) Map of the seafloor in the study area and its surroundings as resulted from merging the available bathymetric datasets. (b) NW-rotated close-up view of the seafloor in the SAFS area (see the rectangle in panel a for the location). Bathymetry color coding is the same as in panel (a). Numbers from 1 to 7 identify the SAFS main segments.

irregular path, and it can be composed of multiple scarps that collectively reach a maximum height of 175 m (Figures 4c and S2, Profiles 12 and 13). SAF4 is a pronounced tectonic lineament, which bounds the western side of the Southern Basin (west side up). The fault scarp associated with SAF4 is quite straight and well developed with a maximum height of 410 m (Figures 4c and S2, Profile 23). SAF4 terminates northward against SAF3. Southward, the data acquired are discontinuous and do not allow for clearly following and mapping the fault scarp associated with SAF4. We thus tentatively associated with SAF4 various geomorphic features, resembling possible fault scarps that are aligned in the ideal southward continuation of its trace. SAF5 delimits the Southern Basin to the east and bounds a structural high named "Snakehead" (marked with a star symbol in Figure 3b). The maximum fault scarp height associated with SAF5 is 210 m (east side up) (Figure S2, Profile 22). The northern termination of SAF5 is close to the southern tip of SAF1, but the relationships between the two faults remain unclear. SAF6 is recognized only in a small sector where high-resolution data are available; nonetheless, it was included in the analysis because of its prominence gained from observations of the seismic reflection profiles (see the next paragraph). SAF7 shows an irregular scarp that bounds the eastern side (west side up) of the Snakehead structural high (Figure 3b). Other minor scarps, probably associated with secondary faults, were observed within the basins, suggesting the activity at the seafloor of a complex fault system in which the major segments are SAF1 and SAF4. The latter runs NW-SE with the western side up. The transition zone between Northern and Southern basins is imaged in the morphobathymetric Profile #20 (Figure 4b). It shows the seafloor sloping down toward the SAF4 scarp and being interrupted only by minor high-relief zones associated with SAF3 and SAF1, which present scarps of reduced height.

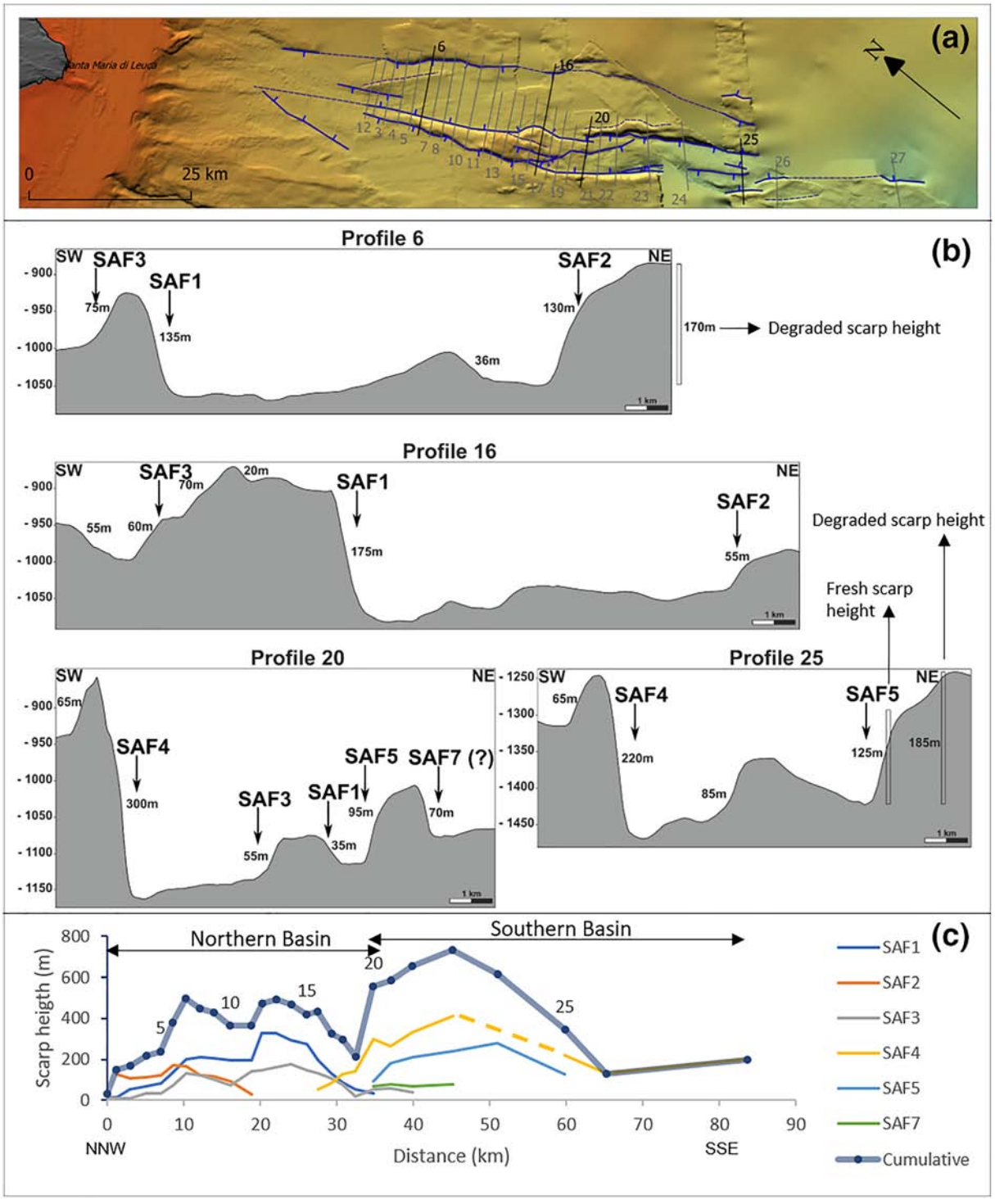

Figure 4. (a) Same map as in Figure 3b with traces of the bathymetric profiles. The profiles shown in panel (b) are those represented by thick black lines. Thin gray lines represent the profiles shown in supporting information Figure S2. (b) Selected bathymetric profiles across the SAFS. Arrows point at the intersection with different SAFS segments. (c) Fault-scarp heights of individual fault segments (colored thin lines, dashed where interpolated, of SAF1-7, Figure 3) correlated across the profiles and aggregated into overall scarp heights of the SAFS (thick blue line with markers indicating the intersected profiles shown in panel a).

Table 3
Description of the Seismic Facies Recognized in the Multichannel Seismic Reflection Profiles (See Supporting Information Table S1 for Details)

Seismic facies	Reflection configuration	Amplitude	Continuity	Frequency	Interpretation	Age
Sf1	Chaotic reflectors. Locally wedge-shaped	Low	Low	Low	Debris and/or turbiditic body	Pleistocene-Holocene
Sf2	Parallel and subparallel reflectors. Locally wedge-shaped clinoforms	Low to moderate	High	High	Prograding wedge and pelagic deposits	Upper Pliocene-Pleistocene-Holocene
Sf3	Mostly transparent with some layering	Low	High	High	Lower Pliocene ("Trubi" equivalent)	Zanclean
Sf4	High-amplitude hummocky reflectors	High	High	High	Chaotic and evaporitic (?) deposits	Messinian
Sf5	Parallel to subparallel reflectors. Locally pinch out	Low	Moderate	Moderate	Siliciclastic marls (Schlier equivalent)	Lower Miocene (?)
Sf6	Parallel to subparallel reflectors. Locally pinch out	High	Moderate to high	Low	Marly and calcarenitic deposits (Bisciaro equivalent)	Oligocene - Lower Miocene (?)
Sf7	Alternation of reflective layers and transparent bodies	Moderate to high	Moderate to high	Low to moderate	Carbonatic multilayer (Maiolica-Scaglia equivalent)	Cretaceous-Eocene (?)
Sf8	Chaotic reflection and locally downlap clinoforms	Moderate to low	Low	Moderate to high	Platform Lower slope	Jurassic-Cretaceous (?)
Sf9	High amplitude hummocky reflectors with onlap of other facies	Moderate to high	Moderate to Low	Low	Platform Escarpment	Jurassic-Cretaceous
Sf10	Hummocky reflectors and sub-transparent seismic facies	Moderate to high	Low	Low	Inner platform	Upper Triassic to Jurassic-Cretaceous
Sf11	Subtransparent seismic facies with locally high-amplitude, low-frequency reflections	Moderate to high	Low	Low	Dolostones and evaporites (Burano Formation). Terrigenous succession (?)	Permian-Triassic (?)

Note. References for the seismic facies and age constraints: Butler (2009, Del Ben et al. (2015), and Volpi et al. (2017).

Overall, the height of the fault scarps associated with the tectonic lineaments varies markedly from north to south. In the northern part (Profiles #1–6 in Figures 4b and S2), the dominant scarp is that associated with SAF2, which is up to 170 m high. From Profile #7 onward, the SAF2 scarp height decreases gradually moving southward, where SAF1 takes its place, becoming the dominant scarp with a maximum elevation of 350 m (Profiles #7–16). Farther south (Profiles #17–20), the seafloor morphology is complicated by the presence of the scarps produced by the overlapping segments of SAF1, SAF3, SAF4, and other minor scarps. In the Southern Basin, the fault scarp associated with SAF4 is even more prominent than the SAF1 scarp (Profiles #20–25), with maximum measured heights of more than 400 m. In the southernmost part of the study area (Profiles #25–27), the high-resolution bathymetry covers only small parts of the fault scarps and does not allow for a complete inspection. The aggregated offset associated with all the scarps of the SAFS shows two maxima (Figure 4c), one in the Northern Basin, characterized by two peaks, and another in the Southern Basin with a progressive reduction in the overlapping zone, south of the Central Horst.

3.2. Seismostratigraphic Model

The interpretation of the multichannel seismic profiles is based on a seismostratigraphic scheme obtained from the correlation between the stratigraphy reported in the available well logs and the observed seismic units (Table 3). The key horizons delimiting the seismic units correspond to lithological changes and unconformities. The identification of the seismic facies is based on the specific configuration of the reflectors, amplitude, continuity, and frequency, as summarized in Table 3. All the available well logs drilled the Apulian platform units, and even if they are located outside the study area (Figure 2), they have been considered for stratigraphic interpretation. The Lieta 1 well, the closest to the study area, was used to tie the seismic profiles (Figure 2d). Overall, six main horizons and two secondary horizons have been identified within the Mesozoic-to-Pleistocene sedimentary succession (see supporting information Table S1). All these seismostratigraphic units and their mutual relationships, together with the general characteristics of the Apulia domain, are displayed in the NW-SE seismic profile of Figure 5.

The Pliocene to Holocene seismic facies exhibits a clinoformal wedge (Sf2) on the continental slope, visible in the western part of the seismic profile of Figure 5. In the distal area Sf2 unit consists of subparallel reflectors that locally can be covered by a chaotic seismic facies (Sf1). Below Sf2, a continuous semitransparent seismic facies (Sf3) was associated with lower Pliocene pelagic deposits of the Trubi Formation. The base

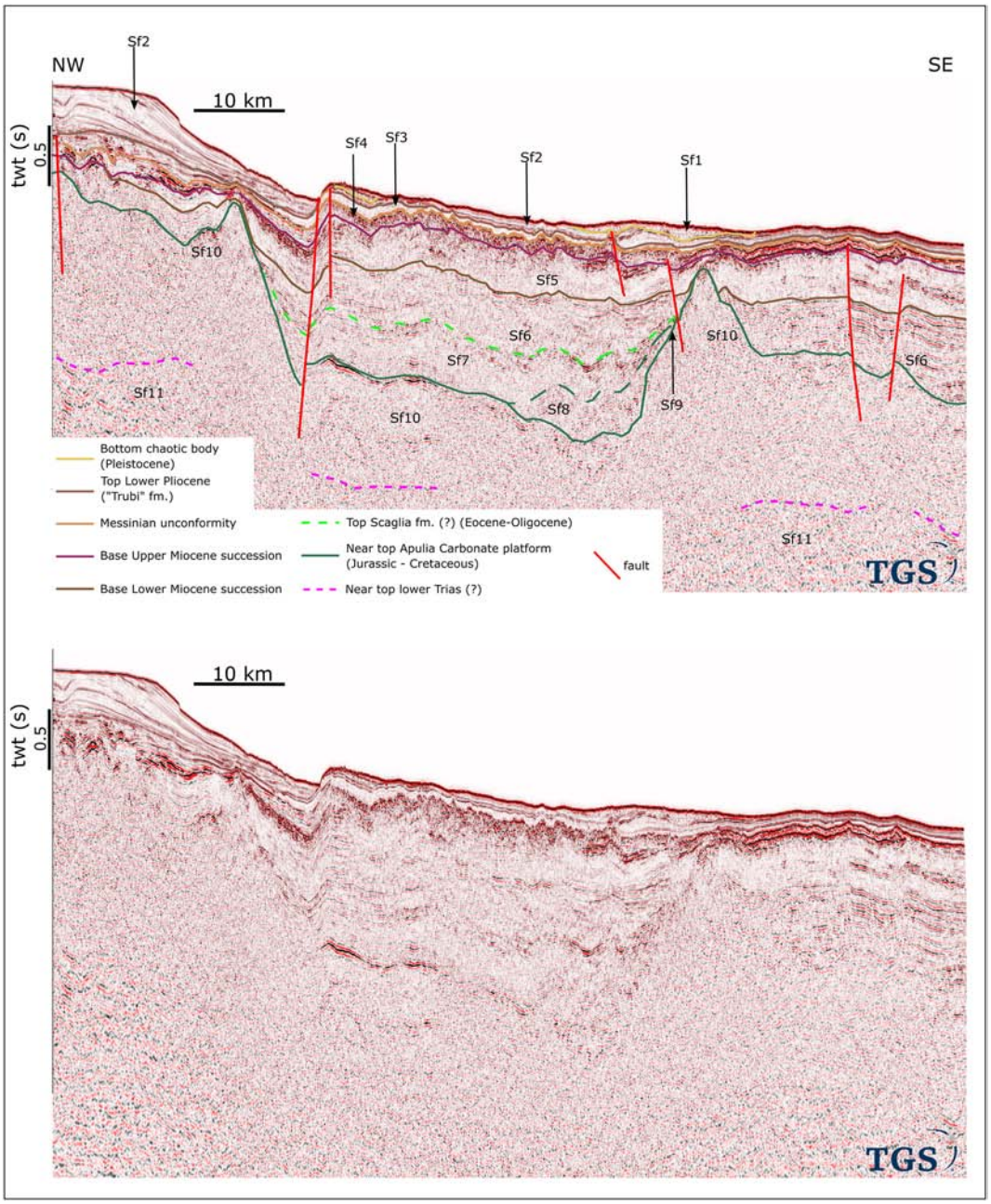

Figure 5. Interpreted (upper panel) and uninterpreted (lower panel) multichannel seismic reflection profiles across the Apulia Swell (see Figure 2a for location). Data courtesy of TGS. See Table 3 for an explanation of seismic facies (Sf) codes in the upper panel. Vertical pseudoexaggeration ~9 times at 3000 m/s default uniform velocity.

of this formation is the Messinian unconformity that is seismically expressed by an undulated, high-amplitude, continuous reflector, generally well recognizable in all seismic profiles. A roughly 70-ms two-way time (TWT) thick (~115 m) succession (Sf4) composed of high- to moderate-amplitude, high-frequency discontinuous reflectors, and with a hummocky geometry, lies below the Messinian unconformity. Sf4 probably consists of evaporitic deposits. Locally, this succession may also show a chaotic aspect. Sf4 overlies a layered seismic unit consisting of an alternation of subparallel moderate to low-amplitude reflectors (Sf5 and Sf6). This succession probably includes the Oligocene-Lower Miocene deposits equivalent of the Bisciaro and Schlier formations as defined in the Central Apennines (Figures 5 and 6 and Table S1). This succession lies on a layered seismic facies consisting of alternating moderate-

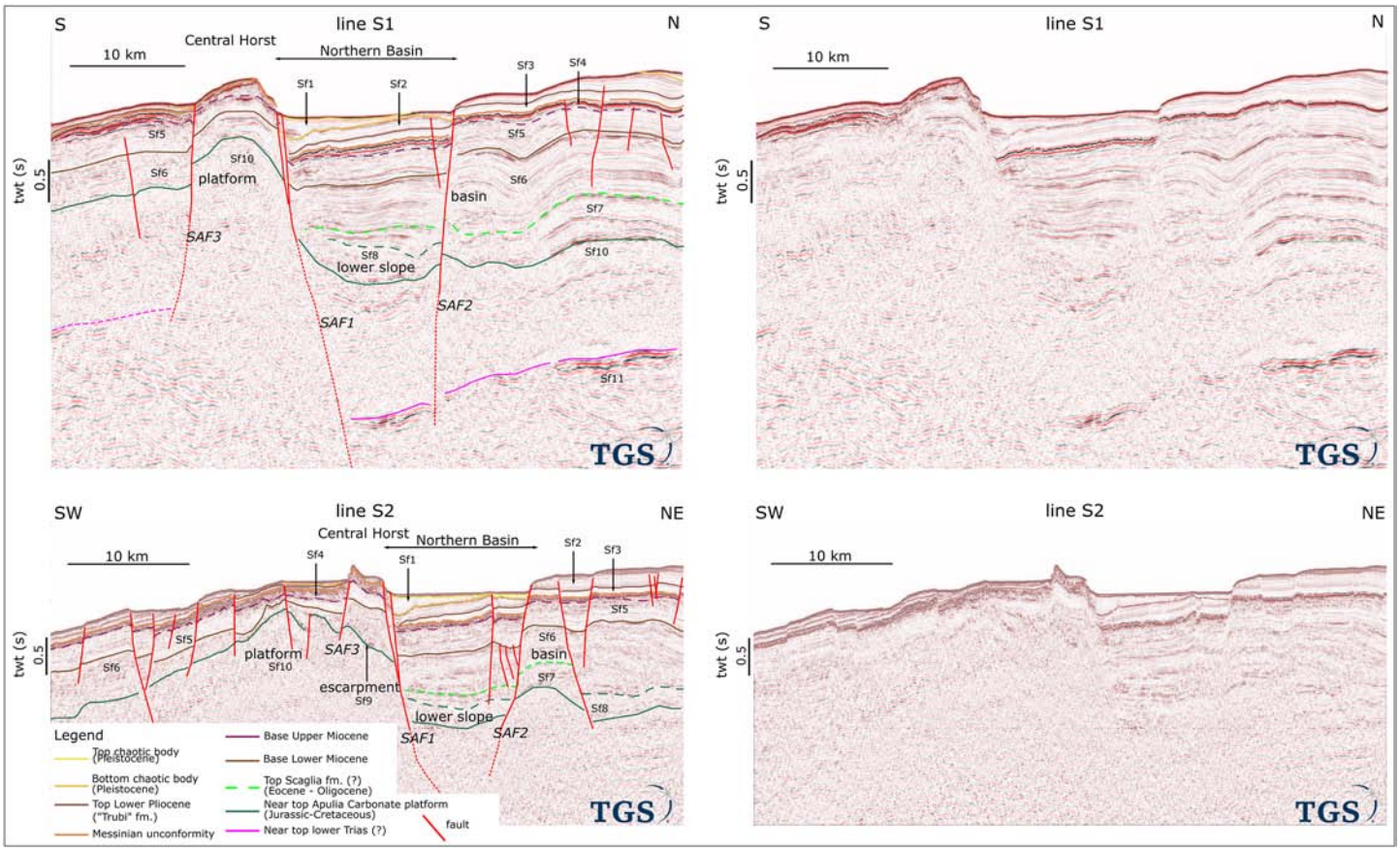

Figure 6. Interpreted (left-hand panel) and uninterpreted (right-hand panel) multichannel Seismic Profiles S1 and S2 (see Figure 2b for location). Data courtesy of TGS. See Table 3 for an explanation of seismic facies (Sf) codes in the left-hand panel. Vertical pseudoexaggeration ~5 times at 3,000-m/s default uniform velocity.

amplitude, high-frequency reflectors here attributed to the Mesozoic-Eocene basinal carbonate deposits of the South Apulia Basin (Sf7). This facies can be observed in the central part of the seismic profile in Figure 5.

Sf7 and Sf6 in Figure 5 pinch-out toward a hummocky and semitransparent seismic facies (Sf10) interpreted as the Apulia carbonate platform succession.

The transition between Sf7 and Sf10 is characterized by onlap terminations against local high-amplitude signals of Sf9, which we interpreted as the platform escarpment marking the gradual transition from the South Apulia Basin to the long-lived Jurassic-to-Miocene carbonate platform. The base of the platform escarpment is characterized by mostly chaotic reflectors with locally recognizable clinoforms, which we interpreted as lower slope deposits (Sf8). The deeper reflectors, analog to Sf10, represent the drowned Jurassic platform whose top is marked by pronounced high-amplitude and low-frequency reflectors.

A high-amplitude and low-frequency set of reflectors are recognizable below Sf10, and we interpreted them as the top of the lower Triassic succession characterized by the presence of evaporites and dolostones (Sf11). Below these reflectors, there is a chaotic seismic facies with occasionally well-resolved reflections, which we interpreted as a possible Permian–Triassic sedimentary succession that has been drilled by Puglia 1 log in northern Apulia (www.videpi.com/deposito/pozzi/profili/pdf/puglia_001.pdf).

3.3. Seismic Interpretation

The structural and depositional elements of the SAFS are imaged in the seismic high-penetration Profiles S1 and S2 from the TGS data set (Figure 6) and in the high-resolution Multichannel Profiles OFS_02, OFS_03, and OFS_04, acquired by OGS (Figure 7). In the following, we will describe the essential observations in each of these profiles.

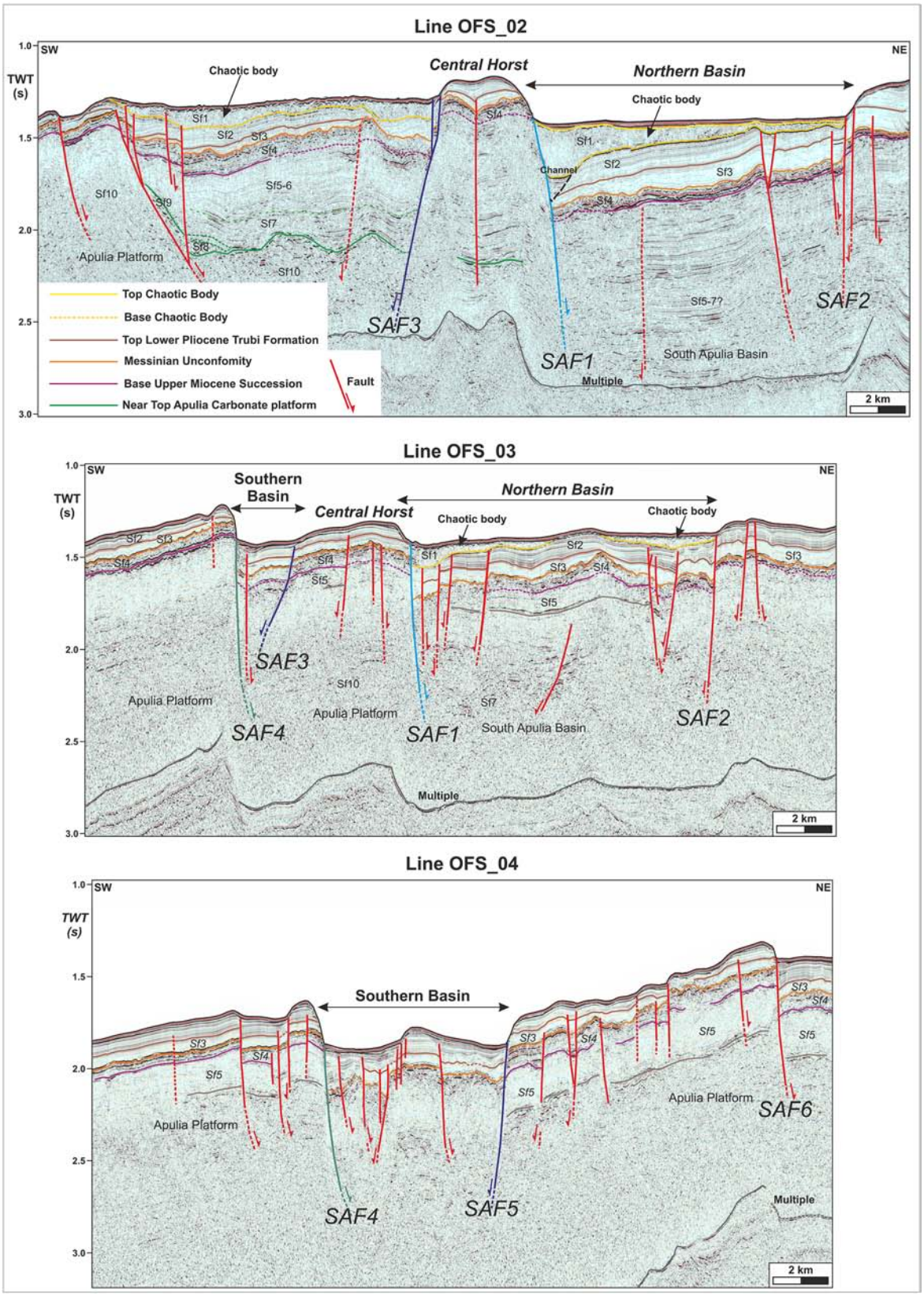

Figure 7. High-resolution multichannel seismic profiles acquired by R/V OGS Explora (see Figure 2b for location, blank version in supporting information Figure S3). Vertical pseudoexaggeration ~5 times at 3,000-m/s default uniform velocity.

3.3.1. Seismic Profiles S1 and S2

Seismic Profiles S1 and S2 in Figure 6 show the same seismic facies observed in the profile of Figure 5 and summarized in Table 3. The corresponding units appear affected by several high-angle normal faults, which control a horst-and-graben configuration. These normal faults were recognized in all the seismic profiles.

The SAFS morphological scarps visible at the seafloor (Figures 3 and 4) are the shallow expression of these faults. This evidence allowed us to correlate the fault segments across various seismic profiles. The graben structure imaged in Profiles S1 and S2 is the Northern Basin, which is delimited by SAF1 to the southwest and SAF2 to the northeast. The hanging wall block within the graben is tilted southward against SAF1. This tilting is particularly evident when looking at the Messinian unconformity. Both the graben-bounding faults seem to reach the seafloor and displace the shallow reflectors of the Pliocene-Holocene units (Sf1 and Sf2). The normal throw of SAF1 measured at the Messinian unconformity is around 700-ms TWT for both Lines S1 and S2.

The Central Horst in line S1 corresponds to a paleogeographic high of the platform unit (Sf10) and is bounded by the southwest dipping SAF3 that reaches the seafloor. This is well evident in the S2 profile, where SAF3 juxtaposes the Miocene pre-Messinian seismic unit (Sf5) in the footwall with the Pliocene-Holocene units (Sf1–3) in the hanging wall, which are possibly affected by a dragging effect near the fault. In this line, the normal vertical offset of the Messinian unconformity measured along SAF3 is around 370-ms TWT. The importance of the main faults bounding the horst-and-graben structure (SAF1, SAF2, and SAF3) can be evaluated by following their downdip extension in the Mesozoic carbonate units. In both Profiles S1 and S2, SAF1 directly juxtaposes the pelagic basin units (Sf6 and Sf7) in the hanging wall with the platform upper margin unit (Sf10) in the footwall. The hanging wall is characterized by the presence of lower-slope deposits with clinoforms and chaotic signals (Sf8). Differently from the profile in Figure 5, Profiles S1 and S2 do not show the gradual transition along the platform escarpment (Sf9); considering that profile S2 is almost orthogonal to SAF1, this anomalous contact of the seismic facies on the two sides of the fault could be ascribed to a horizontal component of motion orthogonal to the section. Within the graben, some minor faults were also identified. The graben infill is characterized by the presence of a package of reflectors with Sf3 facies just above the Messinian unconformity, overlain by Sf2, which is truncated at the top by an unconformity over which we observe the presence of a chaotic body (Sf1) with increasing thickness southward.

The high penetration of these profiles enabled us to reconstruct the geometry of the major elements of the SAFS at least down to the top of the lower Triassic horizon that is well evident to the north of SAF1.

3.3.2. Seismic Profiles OFS_02, OFS_03, and OFS_04

The OFS_02, OFS_03, and OFS_04 seismic profiles (Figure 7, location in Figure 2b), allowed us to describe in more detail the shallow part of the SAFS and to get information on its recent activity.

The southernmost OFS_02 seismic profile crosses the Northern Basin that in this sector is 12 km wide and is filled by a Pliocene-Quaternary succession, up to 390-ms TWT thick, which includes thin and layered Holocene sediments resting on a chaotic body (Sf1) interpreted as a mass-wasting deposit. This chaotic body shows a wedge-shaped growth geometry exhibiting a progressive thickening, from 30- to 260-ms TWT, toward SAF1. The chaotic body lies on a sedimentary succession consisting of an upper sequence made of parallel and continuous reflectors (Sf2), resting onto a lower semitransparent succession (Sf3) associated with the lower Pliocene pelagic Trubi Fm. Below the undulated Messinian unconformity is recognizable a Messinian succession (Sf4), probably lying on the predominantly carbonate basinal deposits of the South Apulia Basin (Sf5–Sf7).

The NE dipping SAF1, developed along the SW side of the Northern Basin, shows a normal vertical displacement of 600-ms TWT at the Messinian unconformity. In the hanging wall block, the tilting of the succession located below the chaotic body toward the SAF1 fault plane is visible. The SE dipping SAF2, developed along the NE side of the basin, shows a normal offset of about 110-ms TWT at the Messinian unconformity. Secondary subvertical normal faults with modest offset are associated with SAF2. A significant high-angle normal fault affects the NE part of the basin infill deforming the base of the chaotic body and probably also the seafloor. Central Horst shows a sedimentary succession similar to the one displayed in the Northern Basin, except for the presence of a thinned Pliocene-Quaternary sequence shaped by the action of currents. The SW margin of the horst is bounded by SAF3, which is characterized in the upper part by two branches

reaching the seafloor. The SW dipping SAF3 is the master fault of the SW basin imaged by the OFS_02 and displaces the Messinian unconformity of about 220-ms TWT. The sedimentary succession of this basin, which resembles the one in the Northern Basin, shows the presence of a significant shallow, chaotic body, up to 95-ms TWT thick, buried below a very thin Holocene draping cover (Sf1). The southern margin of the SW basin is controlled by a NE dipping slightly concave-upward normal fault produced by the merging of three secondary fault planes. This structure develops on the transition between the Apulia Platform and the South Apulia Basin (Sf9 and Sf8) and does not affect the seafloor.

The seismic line OFS_03 crosses the central part of the SAFS, including both the Southern and Northern Basins, separated by the less prominent but wider (4 km) southern portion of the Central Horst. The narrow Southern Basin (less than 2 km wide) starts to develop along the southern side of the Central Horst. It is characterized by a thin Pliocene-Quaternary succession, about 126-ms TWT thick, in which no chaotic bodies are present. A filled channel is observable on the hanging wall side of SAF4. The Messinian succession (Sf4) lies onto a semitransparent succession, probably including the lower Messinian-Mesozoic Sf5, Sf6, Sf7, and Sf10 seismic facies.

The Southern Basin is bounded by the high-angle SAF4 and by the southeastern termination of the SAF3. The latter shows a small displacement and does not seem to affect the seafloor. The former instead produced the high scarp (140 m) that represents the southwestern margin of the basin, and it shows a normal offset of 260-ms TWT at the Messinian unconformity.

The sedimentary succession of the Northern Basin, which is about 11 km wide, shows the southern continuation of the chaotic body visible on the OFS_02. This body is split into two parts and shows an undulating erosional surface at the base. The chaotic body progressively thickens away from the ridge located in the central part of the basin, reaching 114-ms TWT at the SAF1 fault plane. The SAF1 and SAF2 show displacements of 230- and 86-ms TWT, respectively, at the Messinian unconformity. Several normal faults with modest offset, and sealed by the chaotic body, affect the basin infill. SAF1 seems to juxtapose the Apulia Platform (Sf10) with the South Apulia Basin succession (Sf7) at a depth of about 2.3-s TWT.

The southernmost OFS_04 seismic profile orthogonally crosses the Southern Basin; in this sector, the Southern Basin is slightly wider, reaching about 6.5 km, while the Northern Basin is no longer present. Prominent fault scarps, up to 170 m high and associated with SAF4 and SAF5, bound the basin on the southern and northern sides. The Pliocene-Quaternary succession of the Southern Basin is up to 178-ms TWT thick; therefore, it is thicker than in the northern sector of the basin. Both SAF4 and SAF5 reach the seafloor and show a normal displacement of about 300- and 160-ms TWT, respectively, at the Messinian unconformity. The Southern Basin is separated into two subbasins by a small structural high bounded by normal faults with a modest offset, probably affecting the seafloor along the southwestern side of the high. The SW part of the basin shows a more complicated structural setting due to the presence of several normal faults. The SAF6 normal fault, located in the northeastern termination of the line, is associated with a prominent fault scarp. Its displacement is about 184-ms TWT at the Messinian unconformity. The Pliocene-Holocene deposits in the hanging wall are characterized by internal unconformities close to the fault, which might be interpreted as clues of recent activity.

3.3.3. Chirp

In the frame of the Chirp data set, the ENE oriented and 12.5-km-long C2 high-resolution profile (Figures 8 and 2 for location) crosses the northern sector of the Northern Basin. It shows in detail the shallow part of the Central Horst bounded by subvertical fault scarps up to 200 and 70 m high, respectively associated with SAF1 and SAF3. These faults cut the recent sedimentary cover, and locally also the seafloor. This circumstance is testified by the small fault-bounded structural high off the base of the eastern side of the Central Horst. This evidence confirms the recent activity of the SAFS.

A considerable jump in seafloor depth, of about 100-ms TWT, is recognizable between the western and eastern side of the Central Horst. A sedimentary succession up to 20-ms TWT thick is visible in the upper part of the profile. It consists of high-frequency, low- to high-amplitude, continuous, and parallel reflectors, interpreted as the pelagic/hemipelagic recent sedimentary cover. These deposits are locally interrupted by the presence of isolated mound morphologies of different sizes that extend down to the acoustic basement. We interpreted these features as possible coral patches, characterized by an acoustically transparent response due to the high reflectivity of their top, which is a peculiar feature of reef structures.

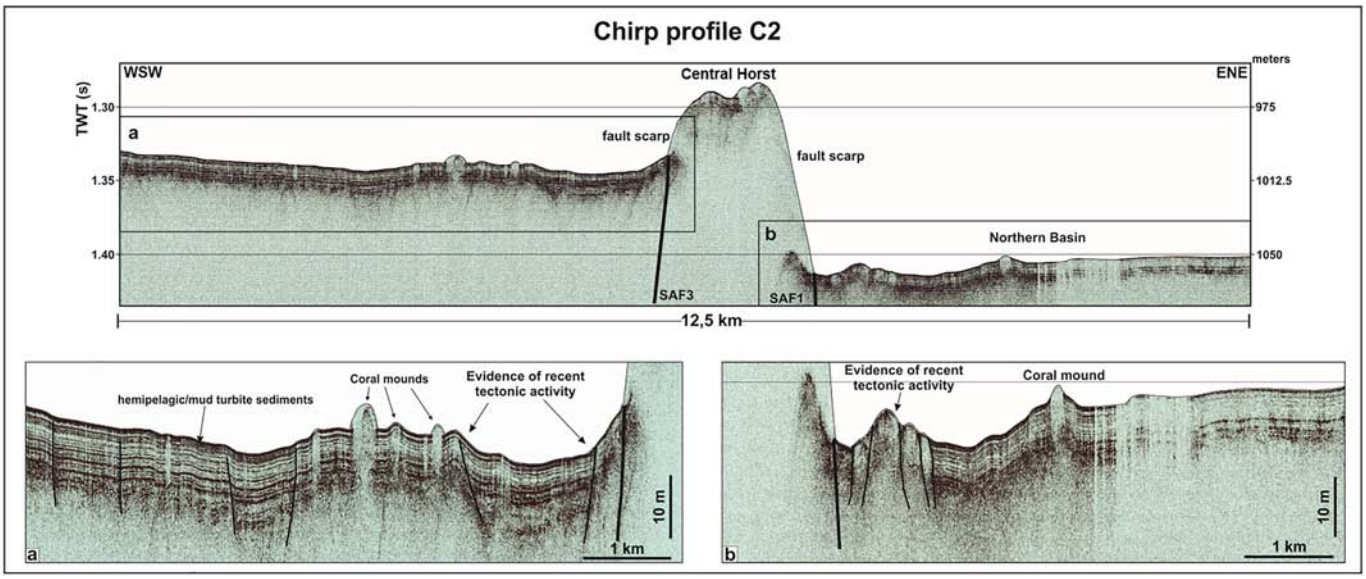

Figure 8. High-resolution subbottom CHIRP C2 (see Figure 2b for location) acquired by R/V OGS Explora. Panels (a) and (b) show two close-up views of the C2 profile in correspondence of SAF3 and SAF1, respectively.

3.4. Isochrone Maps of Key Interfaces

The isochrones maps of the Messinian unconformity and of the top of the Apulia Platform have been produced. The reconstruction of the Messinian unconformity on the Apulia Swell (isochrones in Figure 9a), obtained by interpolating the seismic interpretation, displays a configuration of highs and lows that is consistent with the main features of the seafloor. Within the Northern and Southern Basins, the

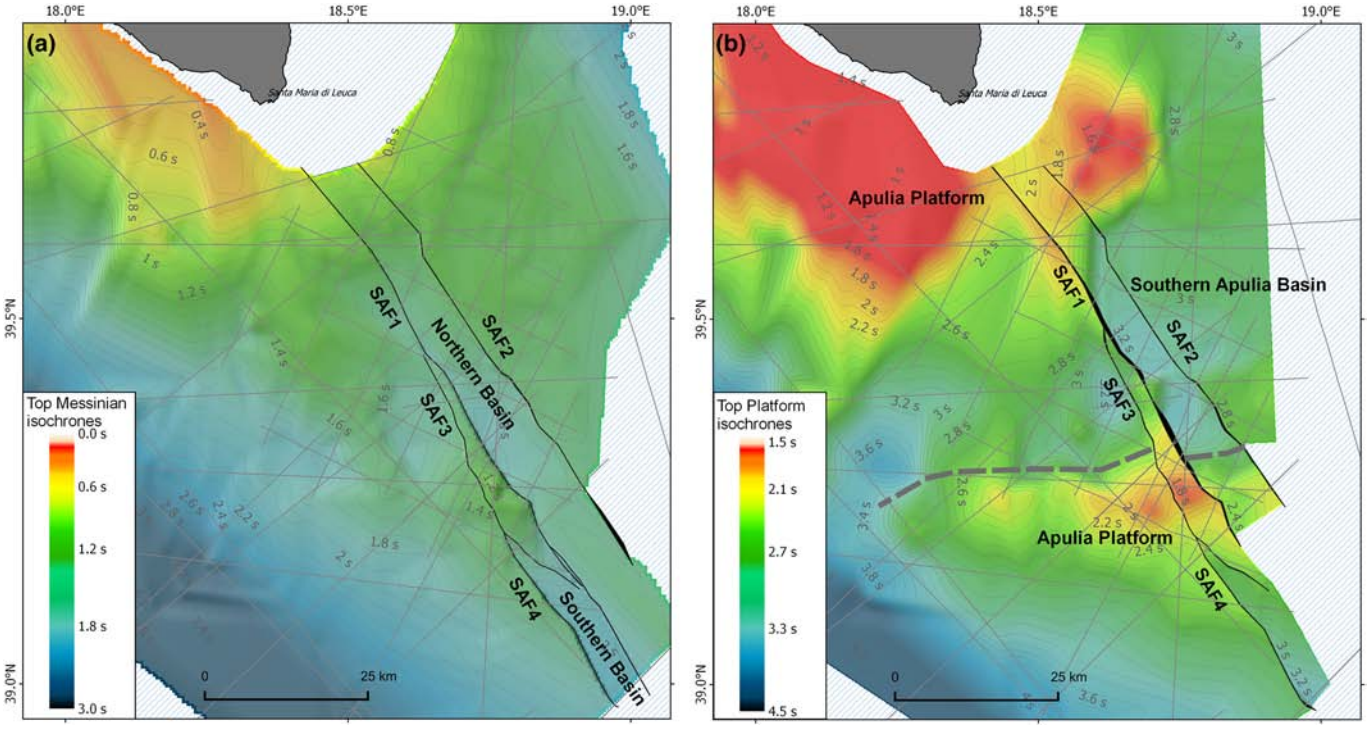

Figure 9. Subsurface isochrone maps derived from the interpretation of multichannel seismic profiles. (a) Top of the Messinian (Messinian unconformity). (b) Top of the Apulia Platform; the gray dashed line represents the local trend of the Apulia Platform Margin.

deepest position of the Messinian unconformity coincides with the main depocenters of the two basins, whereas the Central Horst is the most prominent positive structure. The reconstruction of the top of the Apulia platform (isochrones in Figure 9b) shows an articulated surface generally dipping toward the southwest as an effect of the regional tilt of the Apulia Swell under the Calabrian Arc. Within this general regional trend, the map highlights the presence of the South Apulia Basin in the central part of the study area. The South Apulia Basin is located in between two platform highs to the north and south, the latter being oriented in an E-W direction, also imaged in Figure 5. This paleotopography is dissected obliquely by the SAFS, which locally juxtaposes basin and platform facies along the SAF1.

4. Discussion and Conclusions

We presented the results of an in-depth exploration of the Apulia Swell, a poorly understood area in the central Mediterranean region. Although the tectonic setting suggests that this area should be part of a relatively stable continental region (i.e., the Apulia Foreland) trapped between two confronting chains, we found remarkable evidence of recent (Pliocene-Holocene) tectonic activity epitomized by the SAFS: a 100-km-long, mature, and active fault system, which determined the formation of two elongated basins (Northern Basin and Southern Basin) separated by a prominent horst (Central Horst). The presence of a horst-and-graben structure in the Apulia Swell was already pointed out by several authors. Merlini et al. (2000), Argnani et al. (2001), Finetti and Del Ben (2005), Del Ben et al. (2010), and Milia et al. (2017) mapped some segments of the faults that here we interpreted as being part of the fully fledged SAFS. The mechanism proposed for the formation of these normal faults is the flexure of the forebulge between the Calabrian subduction and the Hellenides collisional thrust belt (Argnani et al., 2001; Billi & Salvini, 2003; Doglioni et al., 1994; Tropeano et al., 2002). Even if this mechanism is plausible to explain such faults as a result of bending-moment extension on a long-wavelength anticlinorium, it would also imply that the identified faults should be short and with limited propagation at depth, possibly to a maximum depth of 2–3 km (Galli & Naso, 2008). The main contribution of this work is that it comes from the analysis and integration of an original multiscale geophysical data set. This allowed us to infer that the previously identified normal faults are the elements of a wider and more articulated regional feature, the SAFS. Besides, our data documented that the series of major faults forming the SAFS extend at least down to 12-km depth (considering the average velocity for the Apulia carbonates proposed in Table 2), reaching the top of the lower Triassic succession and possibly rooting in the Permian-Triassic succession, as deduced by the interpretation of Line S1 (Figure 6).

The horst-and-graben configuration in the Salento Peninsula was already established in the Late Pliocene to Early Pleistocene and the subsequent deposition of the regressive Pleistocene sedimentary cycle postdates the onshore fault activity (Tropeano et al., 2002). Our observations on the SAFS remark that in the investigated offshore sector of the Apulia Swell, the activity of the faults postdates the Late Pliocene deposits and locally controls the deposition in the Northern Basin and Southern Basin. From the viewpoint of the tectonic context of the region, this implies that the SAFS is younger than the faults with a similar orientation observed onshore; thus, it can be considered as a remarkable exception.

Both the multichannel seismic profiles and the high-resolution subbottom CHIRP profile showed that the major faults of the SAFS offset the late Quaternary and Holocene deposits and even affect the seafloor. The high-resolution subbottom CHIRP profile (Figure 8) clearly shows the evidence of recent deformation at the seafloor due to the activity of SAF1 and possibly also of SAF3. Pelagic/hemipelagic Holocene sedimentary drapes record the recent deformation. Locally, these deposits are interrupted by the presence of mound-like features of variable size (100–250 m wide). They appear as isolated bodies cutting the Holocene sedimentary cover and extending downward to the CHIRP acoustic basement. In agreement with Fusi et al. (2006) and Savini and Corselli (2010), we interpreted these features as possible coral mounds, potentially associated with gas escapes, and lying along to fault scarps (Etiope et al., 2010). The analysis of the bathymetric profiles highlights two maxima of the aggregated fault scarp heights, one maximum located in correspondence to the Northern Basin and the other to the Southern Basin (Figure 4c). The height of the fault scarps is controlled by the interaction between the tectonic displacement occurring along the fault and the partial filling of the accommodation space created at its base by the sediment supply. In particular, the analysis of the aggregated fault scarp heights (Figure 4c) suggests a gradual transfer of the deformation

Table 4
Long-Term Sedimentation Rates Measured by Analyzing the Pliocene-Holocene Sequence After Depth Conversion (Figure 10)

Section	Basin	FWT max (m)	FWT min (m)	Sed. rate max (mm/yr)	Sed. rate min (mm/yr)	Sed. rate average (mm/yr)
S2	Northern Basin	412	343	0.078	0.065	0.071
S1-OFS_2	Northern Basin	396	350	0.075	0.066	0.070
OFS_3	Northern Basin	238	213	0.045	0.040	0.043
OFS_3	Southern Basin	162	151	0.031	0.028	0.030
OFS_4	Southern Basin	188	169	0.035	0.032	0.034

Note. FWT: footwall thickness of the post-Messinian succession.

between the two basins. In the Southern Basin, the observed fault scarp reaches the maximum height due to the lower sedimentation rates in the hanging wall, which enhances the appearance of its free surface. Conversely, in the northern sector of the Northern Basin the presence of mass-wasting deposits (Figure 3a), imaged as a chaotic body in the seismic profiles (Figures 6 and 7), compensates the accommodation space created by the progressive southward tilting of the hanging wall block due to the fault activity. Therefore, even if the fault scarps in the Northern Basin are generally less evident, this would not imply that their activity rate is necessarily lower than the activity rate of the faults bounding the Southern Basin. We thus interpreted SAF1 and SAF4 as the major normal fault of the SAFS and the deformation pattern observed in the bathymetry (Figure 3b) as the effect of a relay zone between these two major faults, which produced the migration of the deformation from the Northern Basin to the Southern Basin.

The trend of the SAFS is oblique with respect to the E-W structural trend of the Apulia Carbonate Platform paleomargin, as highlighted by the subsurface reconstruction of the top of the Apulia Platform reported in Figure 9b. This arrangement suggests that the SAFS should have formed and grown after the formation of the Apulia Platform. By analyzing the Pliocene-Holocene sedimentary succession in the seismic profiles, we observe that the reflectors of Sf2 above the Messinian unconformity are subparallel to the unconformity itself and maintain roughly the same thickness also in the footwall of the SAFS toward the northeast (Figure 6, Line S2). The subparallelism of sedimentation layers above the Messinian unconformity is abruptly interrupted by Sf1, a sedimentary wedge characterized by growth strata with onlap terminations against the Sf2 top and chaotic deposits. The growth strata, developed within the Pliocene-Quaternary succession, mark the beginning of the tectonic activity of the faults bounding the Northern Basin. In the absence of any direct prospection (well logs) in this specific area, we thus rely on an indirect estimate to constrain the age of inception of the SAFS and, consequently, of the throw rate of its fault segments. To this end, we assumed that the average thickness of the post-Messinian seismostratigraphic units measured on the footwall of the fault is representative of a long-term average sedimentation rate and that this same rate can be applied to the pretectonic deposits in the fault hanging wall. Therefore, knowing the thickness of pretectonic strata and their estimated sedimentation rate (Table 4), we can calculate the time necessary for their deposition over the Messinian unconformity. Then, subtracting the obtained amount of time from the age of the Messinian unconformity (5.3 Ma) provides a fair estimation of the age of the fault inception. The major limitation of this technique is the unknown amount of pretectonic deposits possibly removed by seafloor processes during the emplacement of the chaotic body within Sf1. We thus assume that our estimate is a maximum boundary for the correct age of inception (i.e., the actual value could be younger than our estimate). Considering this major limitation and other sources of uncertainty, it is recommended to adopt a probabilistic approach in the throw rate calculation, such as the method proposed by Zechar and Frankel (2009). Since throw rates are derived quantities, we consider both the age of inception and the displacement as variables with epistemic uncertainty described by a Gaussian probability density function (PDF) around the average measured values. For each fault segment recognized in more than one seismic profile, the PDFs are obtained by normalizing the sum of the individual measurements for each profile. The results are then combined to show the variability of the throw rate estimates.

The PDF of the age of inception (Figure 10b and Table 5) is derived considering the observed variability in the sedimentation rate in the footwall under the assumption of a long-term constant average sedimentation rate along the profile length. The average long-term sedimentation rates obtained from our calculations

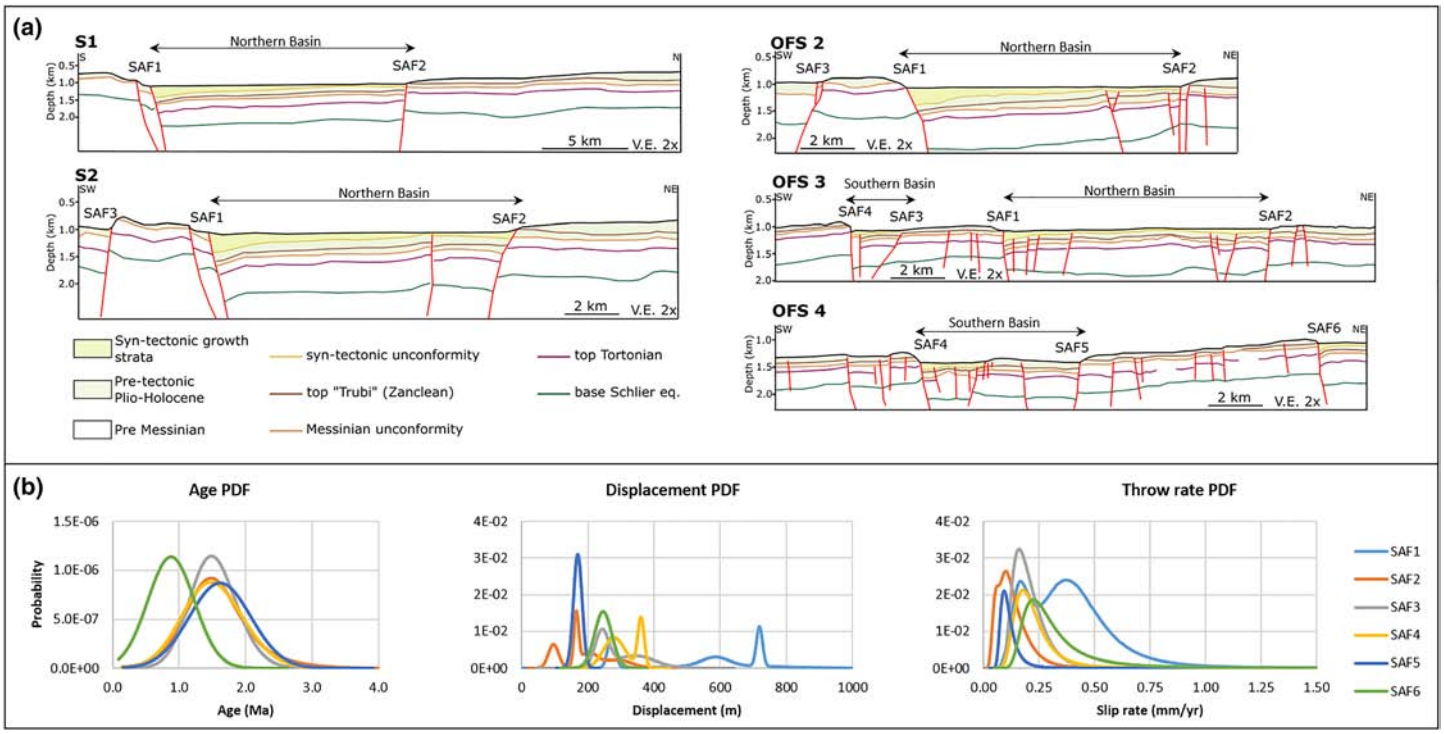

Figure 10. (a) Geological profiles derived from the multichannel seismic profiles (Figures 6 and 7) showing the shallow expression of the SAFS and the control it exerts on the Pliocene-Holocene sediment deposition. (b) Graph showing the probability density functions for the Age of Inception, the displacement, and the throw rate obtained by applying the method proposed by Zechar and Frankel (2009) (Complete tables of throw rate analysis are in supporting information Tables S2–S7). Input data are in Table 5.

(Figure 10a and Table 4) are progressively lower from north to south. The measured rates in Profiles S2 and S1-OFS_02 (~0.07 mm/yr; Northern Basin) are twice as fast as those measured in profile OFS_04 (~0.03 mm/yr; Southern Basin). The transition occurs in the correspondence of Profile OFS_3 (Central Horst). These values are of the same order of magnitude of the sedimentation rates calculated for shallow drillings in the area (D'Antonio et al., 2016), and the trend is in general agreement with the lower sediment supply in

Table 5
Input Data for the Calculation of the Age of Inception (AoI), Throw, and Throw Rate Probability Density Functions (Figure 10 b)

Fault	Section	PTT max (m)	PTT min (m)	AoI mean (Ma)	AoI st. dev. (Ma)	Throw max (m)	Throw min (m)	Throw mean (m)	Throw st. dev. (m)
SAF1	S1	277	210	1.84	0.67	726 (BS)	713 (Mu)	720	9.2
SAF1	S2	292	262	1.41	0.30	739 (Mu)	511 (Mu)	625	161.1
SAF1	OFS_2	277	240	1.63	0.37	615 (Mu)	556 (TZ)	586	41.4
SAF1	OFS_3	180	153	1.39	0.45	281 (Mu)	264 (TZ)	272	12.0
SAF2	S1	277	210	1.84	0.67	219 (Mu)	183 (TZ)	201	25.5
SAF2	S2	292	262	1.41	0.30	319 (Mu)	255 (TZ)	287	45.3
SAF2	OFS2	277	240	1.63	0.37	170 (Mu)	160 (TZ)	165	7.1
SAF2	OFS3	180	153	1.39	0.45	107 (Mu)	85 (TZ)	96	15.6
SAF3	S2	292	262	1.41	0.30	386 (BS)	301 (Mu)	344	60.1
SAF3	OFS2	277	240	1.63	0.37	258 (BS)	229 (Mu)	244	20.5
SAF4	OFS_3	125	109	1.34	0.38	306 (Mu)	259 (TZ)	282	33.2
SAF4	OFS_4	135	113	1.62	0.46	301 (Mu)	256 (TZ)	278	31.7
SAF5	OFS4	135	113	1.62	0.46	180 (Mu)	162 (TZ)	171	12.9
SAF6	OFS_4	152	136	0.88	0.35	265 (Mu)	228 (TZ)	246	25.9

Note. PTT = Pretectonic thickness. Reference horizon cutoffs: BS = bottom Schlier; Mu = Messinian unconformity; TT = top Tortonian; TZ = top "Trubi" Zanclean.

Table 6
Fault Parameters of the Major Structural Elements Composing the SAFS

Fault	Strike	Dip	Min depth (km)	Max depth[a] (km)	Length (km)	Throw rate (mm/yr)	Throw rate st. dev. (mm/yr)
SAF1	330	60	1.1	12	53	0.37	+0.19 −0.18
SAF2	150	75	1.1	10 ([a])	73 (max)	0.12	+0.08 −0.05
SAF3	160	55	1	10 ([a])	41	0.16	+0.08 −0.05
SAF4	325	66	1.4	12 ([a])	61	0.20	+0.10 −0.05
SAF5	145	70	1.4	—([a])	26 (min)	0.11	+0.04 −0.02
SAF6	325	75	1.1	—	—	0.28	+0.18 −0.08
SAF7	320	70	1.3	—	13	0.04–0.08[b]	—

[a]Value inferred from Seismic Profile S1 that represents a minimum for the maximum possible depth of SAF1. The same value is attributed to SAF4 that is the other master fault of the SAFS.
[b]Value calculated only based on the bathymetric profile (Figure 4) assigning a time interval of activity between 1.62 and 0.88 Ma derived from the information on the neighboring SAF5 and SAF6, respectively.

the distal region, considering that the major source of sediment is located to the north of the Apulia Swell (the current slope area of the Salento Peninsula). Our results suggest that the SAFS segments activated between 1.3 and 1.8 Ma except for the SAF6 segment, which was observed only in a single profile where the analysis of syntectonic deposits suggests a younger age of inception of 0.88 Ma (Table 5). The PDF of the fault displacement (Figure 10b and Table 5) is derived considering the measurements of the average displacement of two or more reference horizon cutoffs and their associated standard deviation in each profile. The values obtained from the analysis of 2-D multichannel surveys and of the PDFs are shown in Table 5. The resulting throw rates and their associated uncertainty are reported in Table 6, and their PDF is shown in Figure 10b. The major fault controlling the Northern Basin is SAF1, for which we obtained a throw rate of 0.37 mm/yr with an age of inception of 1.3–1.8 Ma. The major fault controlling the Southern Basin is SAF4, whose age of inception is constrained in the interval 1.3–1.6 Ma, slightly younger than that of SAF1, and has a throw rate of 0.20 mm/yr. Future studies should focus on more robust constraints of the fault inception ages, which have higher uncertainty, to improve these throw rate estimates. A borehole within either basin controlled by the SAFS would be essential to overcome the difficulties posed by the uncertainty of the long-term sedimentation rate in the area. More specifically, better data would be needed for SAF1, whose throw rate PDF is bimodal and wider than all the others.

The dip-slip component of the SAFS activity in the upper crust is predominant and well documented by both the morphobathymetric and the seismic reflection data. Nonetheless, the evidence of a possible horizontal component of motion is not negligible and needs to be comprehended from a broader perspective. The structural analysis of the Quaternary fracture systems affecting the Salento Peninsula suggests a dominant extensional tectonic regime. This might be characterized by triaxial stress during Early and Middle Pleistocene (Di Bucci et al., 2011) in which a change of the vertical stress axis between $\sigma 1$ and $\sigma 2$ cannot be ruled out. This change would be compatible with the development of transtensive structures. Strike-slip faulting in the larger Apulia region is documented in its northern part along the MGF (Brankman & Aydin, 2004; Favali et al., 1993; Funiciello et al., 1988; Tondi et al., 2005) and was hypothesized by Gambini and Tozzi (1996) in the Salento Peninsula. Right-lateral component of movement on E-W trending faults affecting the Apulia region was also associated with several crustal earthquakes (Fracassi & Valensise, 2007; Fracassi et al., 2012). However, what is the evidence of transtension in the Apulia Swell? The different thickness of the Meso-Cenozoic succession in Line S2 across SAF1, at the contact between basin and platform facies, could suggest a horizontal component of movement almost orthogonal to the section. Moreover, the right-stepping arrangement of SAF1 and SAF4 (Figure 3b) can be interpreted as the result of the activity of a deep-seated left-lateral shear zone in a transtensive tectonic context, as suggested by field observations in other parts of the world and experimental models (Richard et al., 1995; Robson et al., 2018; Rotevatn &

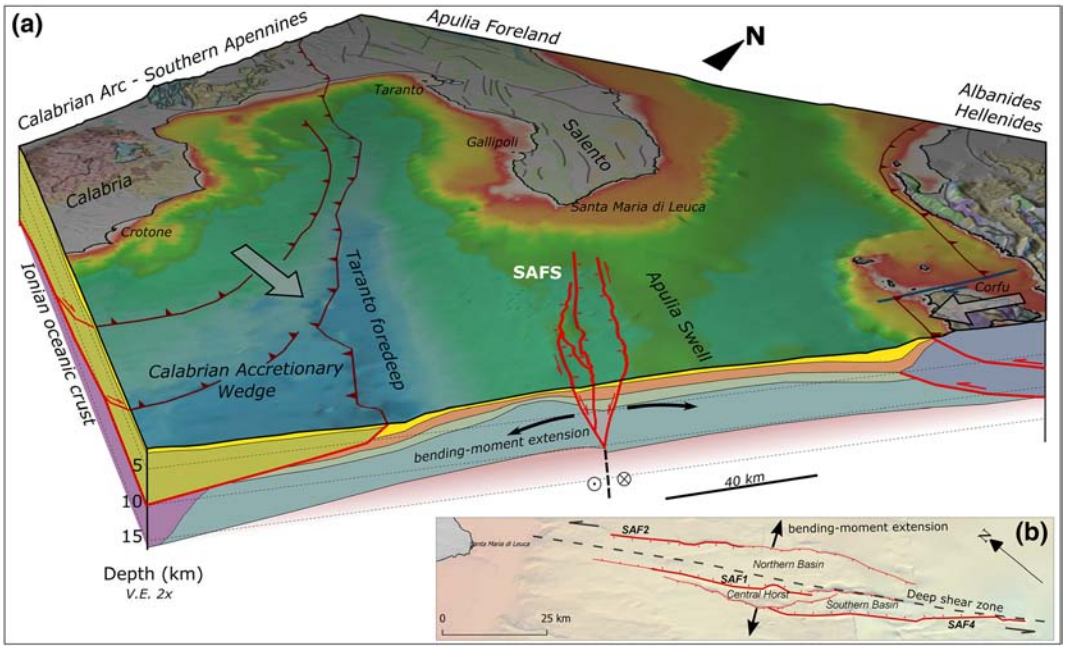

Figure 11. (a) Three-dimensional geological scheme of the SAFS. The color legend is as in Figure 1. Gray arrows represent the regional convergence of the Calabrian Arc and the Albanides-Hellenides. (b) Close-up view of the SAFS area with structural interpretation (see Figure 3a for the location).

Peacock, 2018). The presence of a left-lateral component along the SAFS would be in agreement with the few focal mechanisms recorded in the area. Indeed, the largest earthquake (*Mw* 5.02) of the 1974 seismic sequence (Rovida et al., 2016) had a focal mechanism (Figure 1c), which indicate a left-lateral slip on the NW-SE nodal planes (Favali et al., 1990; Muço, 1994). The seismic sequence of 2013–2014 had the largest earthquake of magnitude Mw 4.06 with an extensional centroid moment tensor (Figure 1c) with a small left lateral component along NW-SE oriented plane (Pondrelli & Salimbeni, 2006). The offshore location of both seismic sequences implies that the hypocenter depths are not well constrained; nonetheless, these sequences confirm the presence of a left-lateral component of motion along planes which share the same orientation with the SAFS master faults.

A hypothesis to explain a horizontal component of motion of the SAFS is that the Apulia Swell could be affected by an extensional regime in the upper crust and by an inner arc contraction in the lower crust (Argnani et al., 2001). These two concurrent processes are the results of the SE convergence of the Calabrian Arc and the WSW convergence of the Hellenides block, both overprinting the regional Africa-Europe convergence and producing the bending moment that controls the Apulia Swell flexure. According to Argnani et al. (2001), the reorientation of the stress axis in the lower crust would produce a horizontal maximum stress and a vertical intermediate stress, leading to a transcurrent stress regime. The orientation of the horizontal stress could reflect the different directions of convergence of the two chains and may be the cause of the hypothesized left-lateral component of the SAFS movement (Figure 11). Except for the few focal mechanisms of the 1974 and 2014 seismic sequences, currently, there are no independent constraints to validate this hypothesis. Therefore, the full kinematic description of the SAFS requires further investigations and a more detailed seismological and geodetic characterization.

Apart from the unsettled points illustrated above, the improved geometrical reconstruction and the kinematic analysis allowed us to provide a comprehensive parametric representation of the SAFS (Table 6). Here, we assume that the calculated throw rates are a good approximation for the actual (rake-parallel) slip rates of the SAFS because its dip-slip kinematics predominates. These results can already be incorporated into the collections of active and seismogenic faults oriented at contributing to earthquake hazard studies and models. In this respect, a compelling implication of the SAFS activity concerns its potential role as the source of the 1743 earthquake. The occurrence of this earthquake, testified by historical records,

signifies that the southern end of the Adria microplate is capable of hosting earthquakes as large as $M \sim 7$. Earthquakes of this magnitude size or larger are not unusual in stable continental regions, even in areas much further away from plate boundaries than the Apulia Swell, and represent a very elusive source of seismic risk (Albini et al., 2019; Calais et al., 2016; England & Jackson, 2011). Until now, the hypotheses about the source of this earthquake fell for different reasons onto a reverse fault, despite the presence of normal faults in the area. Both Argnani et al. (2001) and Galli and Naso (2008) ascribed the 1743 earthquake to a still unknown deep reverse fault related to contraction at depth in the Apulia Swell. Conversely, Milia et al. (2017) maintained that the normal faults of the Apulia Swell are no longer active and concentrated their attention on the only known active fault in the vicinity of the earthquake epicenter, that is, the Corfu Thrust. Although, there are no certain elements (i.e., geologic coseismic information) to assess which fault could have ruptured to generate the 1743 earthquake, the location, the size, and the tectonic activity of the SAFS together form a strong body of facts to start considering it among the most plausible candidates for the source of that earthquake. We hope our data could foster in-depth studies toward a better understanding of an earthquake that plays a key role in the earthquake hazard assessment of the region.

Data Availability Statement

The data analyzed in this study were obtained from TGS, under a nonexclusive confidentiality agreement and from CNR-ISMAR under the payment of a fee. Requests to access these data sets should be directed to TGS (https://www.tgs.com/) and to CNR-ISMAR (http://www.crop.cnr.it/). The bathymetric metadata and Digital Terrain Model data products were derived from the EMODnet Bathymetry portal (http://www.emodnet-bathymetry.eu).

Acknowledgments

This work was carried out in the framework of the project FASTMIT (FAglie Sismogeniche e Tsunamigeniche nei Mari ITaliani) funded by the Italian Ministry for Education, University, and Research (MIUR), Premiale 2014 D. M. 291 03/05/2016. We thank TGS for providing seismic data and also acknowledge IHS Markit Ltd for providing the educational license of the Kingdom Suite Software. We thank the Associate Editor Paola Vannucchi, David Iacopini, and Salvatore Critelli for the constructive comments.

References

Albini, P., Musson, R. M. W., Rovida, A., Locati, M., Gomez Capera, A. A., & Viganò, D. (2019). The global earthquake history. *Earthquake Spectra*, *30*(2), 607–624. https://doi.org/10.1193/122013eqs297

Argnani, A., Frugoni, F., Cosi, R., Ligi, M., & Favali, P. (2001). Tectonics and seismicity of the Apulian Ridge south of Salento peninsula (Southern Italy). *Annals of Geophysics*, *44*(3). https://doi.org/10.4401/ag-3573

Billi, A., Gambini, R., Nicolai, C., & Storti, F. (2007). Neogene-Quaternary intraforeland transpression along a Mesozoic platform-basin margin: The Gargano fault system, Adria, Italy. *Geosphere*, *3*(1), 1. https://doi.org/10.1130/ges00057.1

Billi, A., & Salvini, F. (2003). Development of systematic joints in response to flexure-related fibre stress in flexed foreland plates: The Apulian forebulge case history, Italy. *Journal of Geodynamics*, *36*(4), 523–536. https://doi.org/10.1016/S0264-3707(03)00086-3

Brankman, C. M., & Aydin, A. (2004). Uplift and contractional deformation along a segmented strike-slip fault system: The Gargano Promontory, southern Italy. *Journal of Structural Geology*, *26*(5), 807–824. https://doi.org/10.1016/j.jsg.2003.08.018

Butler, R. (2009). Relationships between the Apennine thrust belt, foredeep and foreland revealed by marine seismic data, offshore Calabria. *Italian Journal of Geosciences*, *128*(2), 269–278. https://doi.org/10.3301/IJG.2009.128.2.269

Calais, E., Camelbeeck, T., Stein, S., Liu, M., & Craig, T. J. (2016). A new paradigm for large earthquakes in stable continental plate interiors. *Geophysical Research Letters*, *43*, 10,621–610,637. https://doi.org/10.1002/2016gl070815

Catalano, R., Doglioni, C., & Merlini, S. (2000). On the Mesozoic Ionian Basin. *Geophysical Journal International*, *143*, 1–24.

Ciaranfi, N., Pieri, P., & Ricchetti, G. (1988). Note alla Carta Geologica delle Murge e del Salento (Puglia centromeridionale). *Memorie della Società Geologica Italiana*, *41*, 449–460.

Critelli, S. (2018). Provenance of Mesozoic to Cenozoic circum-Mediterranean sandstones in relation to tectonic setting. *Earth-Science Reviews*, *185*, 624–648. https://doi.org/10.1016/j.earscirev.2018.07.001

Critelli, S., Muto, F., Perri, F., & Tripodi, V. (2017). Interpreting provenance relations from sandstone detrital modes, southern Italy foreland region: Stratigraphic record of the Miocene tectonic evolution. *Marine and Petroleum Geology*, *87*, 47–59. https://doi.org/10.1016/j.marpetgeo.2017.01.026

D'Antonio, M., Mariconte, R., Arienzo, I., Mazzeo, F. C., Carandente, A., Perugini, D., et al. (2016). Combined Sr-Nd isotopic and geochemical fingerprinting as a tool for identifying tephra layers: Application to deep-sea cores from Eastern Mediterranean Sea. *Chemical Geology*, *443*, 121–136. https://doi.org/10.1016/j.chemgeo.2016.09.022

Del Ben, A. (2009). Earthquakes and shallow structures in South Adria: Evidence of recent inversion tectonics. In P. Guarnieri (Ed.), *Recent progress on earthquake geology*, *Environmental Science, Engineering and Technology Series* (pp. 147–163). New York: Nova Science Publisher, Inc.

Del Ben, A., Geletti, R., & Mocnik, A. (2010). Relation between recent tectonics and inherited Mesozoic structures of the central-southern Adria plate. *Bollettino di Geofisica Teorica ed Applicata*, *51*.

Del Ben, A., Mocnik, A., Volpi, V., & Karvelis, P. (2015). Old domains in the South Adria plate and their relationship with the West Hellenic front. *Journal of Geodynamics*, *89*, 15–28. https://doi.org/10.1016/j.jog.2015.06.003

Di Bucci, D., Caputo, R., Mastronuzzi, G., Fracassi, U., Selleri, G., & Sansò, P. (2011). Quantitative analysis of extensional joints in the southern Adriatic foreland (Italy), and the active tectonics of the Apulia region. *Journal of Geodynamics*, *51*(2–3), 141–155. https://doi.org/10.1016/j.jog.2010.01.012

Doglioni, C., Merlini, S., & Cantarella, G. (1999). Foredeep geometries at the front of the Apennines in the Ionian Sea (central Mediterranean). *Earth and Planetary Science Letters*, *168*(3-4), 243–254. https://doi.org/10.1016/S0012-821X(99)00059-X

Doglioni, C., Mongelli, F., & Pieri, P. (1994). The Puglia uplift (SE Italy): An anomaly in the foreland of the Apenninic subduction due to buckling of a thick continental lithosphere. *Tectonics*, *13*(5), 1309–1321. https://doi.org/10.1029/94TC01501

England, P., & Jackson, J. (2011). Uncharted seismic risk. *Nature Geoscience*, *4*(6), 348–349. https://doi.org/10.1038/ngeo1168

Etiope, G., Savini, A., Lo Bue, N., Favali, P., & Corselli, C. (2010). Deep-sea survey for the detection of methane at the "Santa Maria di Leuca" cold-water coral mounds (Ionian Sea, South Italy). *Deep Sea Research Part II: Topical Studies in Oceanography*, *57*(5–6), 431–440. https://doi.org/10.1016/j.dsr2.2009.08.020

Favali, P., Funiciello, R., Mattietti, G., Mele, G., & Salvini, F. (1993). An active margin across the Adriatic Sea (central Mediterranean Sea). *Tectonophysics*, *219*(1-3), 109–117. https://doi.org/10.1016/0040-1951(93)90290-Z

Favali, P., Mele, G., & Mattietti, G. (1990). Contribution to the study of the Apulian microplate geodynamics. *Memorie della Società Geologica Italiana*, *44*, 71–80.

Finetti, I. R., & Del Ben, A. (2005). Crustal tectono-stratigraphic setting of the Adriatic Sea from new CROP seismic data. In I. R. Finetti (Ed.), *CROP PROJECT: Deep seismic exploration of the Central Mediterranean and Italy* (pp. 519–547). Amsterdam: Elsevier Science.

Fracassi, U., Di Bucci, D., Ridente, D., Trincardi, F., & Valensise, G. (2012). Recasting historical earthquakes in coastal areas (Gargano Promontory, Italy): Insights from marine paleoseismology. *Bulletin of the Seismological Society of America*, *102*(1), 1–17. https://doi.org/10.1785/0120110001

Fracassi, U., & Valensise, G. (2007). Unveiling the sources of the catastrophic 1456 multiple earthquake: Hints to an unexplored tectonic mechanism in southern Italy. *Bulletin of the Seismological Society of America*, *97*(3), 725–748. https://doi.org/10.1785/0120050250

Funiciello, R., Montone, P., Salvini, F., & Tozzi, M. (1988). Caratteri strutturale del promontorio del Gargano. *Memorie della Società Geologica Italiana*, *41*, 1235–1243.

Fusi, N., Savini, A., & Corselli, C. (2006). Evidence of mud diapirism and coral colonies in the Ionian Sea (central Mediterranean) from high resolution chirp sonar survey. *Annals of Geophysics*, *49*, 751–765.

Galli, P., & Naso, G. (2008). The "taranta" effect of the 1743 earthquake in Salento (Apulia, southern Italy). *Bollettino di Geofisica Teorica ed Applicata*, *49*(2), 177–204.

Gambini, R., & Tozzi, M. (1996). Tertiary geodynamic evolution of the southern Adria microplate. *Terra Nova*, *8*(6), 593–602. https://doi.org/10.1111/j.1365-3121.1996.tb00789.x

Guidoboni, E., Ferrari, G., Tarabusi, G., Sgattoni, G., Comastri, A., Mariotti, D., et al. (2019). CFTI5Med, the new release of the catalogue of strong earthquakes in Italy and in the Mediterranean area. *Sci Data*, *6*(1), 80. https://doi.org/10.1038/s41597-019-0091-9

ISIDe Working Group (2007), Italian Seismological Instrumental and Parametric Database (ISIDe), edited. https://doi.org/10.13127/ISIDE

Locati, M., Camassi, R. D., Rovida, A. N., Ercolani, E., Bernardini, F. M. A., Castelli, V., et al. (2016). DBMI15, the 2015 version of the Italian Macroseismic Database, edited, Istituto Nazionale di Geofisica e Vulcanologia. https://doi.org/10.6092/INGV.IT-DBMI15

Maesano, F. E., & D'Ambrogi, C. (2017). Vel-IO 3D: A tool for 3D velocity model construction, optimization and time-depth conversion in 3D geological modeling workflow. *Computers & Geosciences*, *99*, 171–182. https://doi.org/10.1016/j.cageo.2016.11.013

Maesano, F. E., Tiberti, M. M., & Basili, R. (2017). The Calabrian Arc: Three-dimensional modelling of the subduction interface. *Scientific Reports*, *7*(1), 8887. https://doi.org/10.1038/s41598-017-09074-8

Mastronuzzi, G., Pignatelli, C., Sansò, P., & Selleri, G. (2007). Boulder accumulations produced by the 20th of February, 1743 tsunami along the coast of southeastern Salento (Apulia region, Italy). *Marine Geology*, *242*(1–3), 191–205. https://doi.org/10.1016/j.margeo.2006.10.025

Merlini, S., Cantarella, G., & Doglioni, C. (2000). On the seismic profile Crop M5 in the Ionian Sea. *Bollettino-Societa Geologica Italiana*, *119*(2), 227–236.

Milia, A., Iannace, P., & Torrente, M. M. (2017). Active tectonic structures and submarine landslides offshore southern Apulia (Italy): A new scenario for the 1743 earthquake and subsequent tsunami. *Geo-Marine Letters*, *37*(3), 229–239. https://doi.org/10.1007/s00367-017-0493-7

Minelli, L., & Faccenna, C. (2010). Evolution of the Calabrian accretionary wedge (central Mediterranean). *Tectonics*, *29*, TC4004. https://doi.org/10.1029/2009tc002562

Moretti, I., & Royden, L. (1988). Deflection, gravity anomalies and tectonics of doubly subducted continental lithosphere: Adriatic and Ionian Seas. *Tectonics*, *7*(4), 875–893. https://doi.org/10.1029/TC007i004p00875

Muço, B. (1994). Focal mechanism solutions for Albanian earthquakes for the years 1964–1988. *Tectonophysics*, *231*(4), 311–323. https://doi.org/10.1016/0040-1951(94)90041-8

Nappi, R., Gaudiosi, G., Alessio, G., De Lucia, M., & Porfido, S. (2017). The environmental effects of the 1743 Salento earthquake (Apulia, southern Italy): A contribution to seismic hazard assessment of the Salento Peninsula. *Natural Hazards*, *86*(S2), 295–324. https://doi.org/10.1007/s11069-016-2548-x

Nicolai, C., & Gambini, R. (2007). Structural architecture of the Adria platform-and-basin system. *Bollettino della Società Geologica Italiana*, *7*, 21–37.

Pondrelli, S., and S. Salimbeni (2006), Italian CMT Dataset [Data set]. Istituto Nazionale di Geofisica e Vulcanologia (INGV). https://doi.org/10.13127/rcmt/italy

Ricchetti, G., Ciaranfi, N., Luperto Sinni, E., Mongelli, F., & Pieri, P. (1988). Geodinamica ed evoluzione sedimentaria e tettonica dell'avanpaese Apulo. *Memorie della Società Geologica Italiana*, *41*, 57–82.

Richard, P. D., Naylor, M. A., & Koopman, A. (1995). Experimental models of strike-slip tectonics. *Petroleum Geoscience*, *1*(1), 71–80. https://doi.org/10.1144/petgeo.1.1.71

Robson, A. G., Holford, S. P., King, R. C., & Kulikowski, D. (2018). Structural evolution of horst and half-graben structures proximal to a transtensional fault system determined using 3D seismic data from the Shipwreck Trough, offshore Otway Basin. *Australia, Marine and Petroleum Geology*, *89*, 615–634. https://doi.org/10.1016/j.marpetgeo.2017.10.028

Rotevatn, A., & Peacock, D. C. P. (2018). Strike-slip reactivation of segmented normal faults: Implications for basin structure and fluid flow. *Basin Research*, *30*(6), 1264–1279. https://doi.org/10.1111/bre.12303

Rovida, A., Locati, M., Camassi, R., Lolli, B., & Gasperini, P. (Eds.) (2016). Catalogo Parametrico dei Terremoti Italiani (CPTI15). Istituto Nazionale di Geofisica e Vulcanologia (INGV). https://doi.org/10.6092/INGV.IT-CPTI15

Savini, A., & Corselli, C. (2010). High-resolution bathymetry and acoustic geophysical data from Santa Maria di Leuca Cold Water Coral province (Northern Ionian Sea-Apulian continental slope). *Deep Sea Research Part II: Topical Studies in Oceanography*, *57*(5-6), 326–344. https://doi.org/10.1016/j.dsr2.2009.08.014

Teofilo, G., Antoncecchi, I., & Caputo, R. (2018). Neogene-Quaternary evolution of the offshore sector of the Southern Apennines accretionary wedge, Gulf of Taranto, Italy. *Tectonophysics*, *738-739*, 16–32. https://doi.org/10.1016/j.tecto.2018.05.006

Tondi, E., Piccardi, L., Cacon, S., Kontny, B., & Cello, G. (2005). Structural and time constraints for dextral shear along the seismogenic Mattinata Fault (Gargano, southern Italy). *Journal of Geodynamics*, *40*(2–3), 134–152. https://doi.org/10.1016/j.jog.2005.07.003

Tropeano, M., Sabato, L., & Pieri, P. (2002). Filling and cannibalization of a foredeep: the Bradanic Trough, Southern Italy. *Geological Society, London, Special Publications*, *191*(1), 55–79. https://doi.org/10.1144/gsl.sp.2002.191.01.05

Volpi, V., Accettella, D., & Cuppari, A. (2011). Morphological features of the Apennines foreland/accretionary-wedge boundary in the Ionian Sea. *Marine Geophysical Research*, *32*(4), 481–492. https://doi.org/10.1007/s11001-011-9140-2

Volpi, V., Del Ben, A., Civile, D., & Zgur, F. (2017). Neogene tectono-sedimentary interaction between the Calabrian Accretionary Wedge and the Apulian Foreland in the northern Ionian Sea. *Marine and Petroleum Geology*, *83*, 246–260. https://doi.org/10.1016/j.marpetgeo.2017.03.013

Zechar, J. D., & Frankel, K. L. (2009). Incorporating and reporting uncertainties in fault slip rates. *Journal of Geophysical Research*, *114*, B12407. https://doi.org/10.1029/2009jb006325